KASTAMONU UNIVERSITY JOURNAL OF ENGINEERING AND SCIENCES

e-ISSN 2667-8209

VOL: 10 ISSUE: 01

KASTAMONU UNIVERSITY JOURNAL OF ENGINEERING AND SCIENCES

e-ISSN 2667-8209

Kastamonu University Journal of Engineering and Science

Kastamonu University Journal of Engineering and Science publish as blind peer review and two times in a year.

Kastamonu University
Journal of Engineering and Science

Vol: 10 Issue: 1 June 2024 E-ISSN:2667-8209

Kastamonu University
Journal of Engineering and Science

Vol: 10 Issue: 1 June 2024 E-ISSN:2667-8209

Kastamonu University Faculty of Engineering and Architecture 37150 Kastamonu / TÜRKİYE
Tel: +(90)366 2802901 Fax: +(90)366 2802900

Web: https://dergipark.org.tr/tr/pub/kastamonujes
e-mail: kujes@kastamonu.edu.tr

This journal is published two times in a year.
June and December
Kastamonu University Journal of Engineering and Science
Indexed and Abstracted in: Dergipark

Kastamonu University
Journal of Engineering and Science

Vol: 10 Issue: 1 June 2024 E-ISSN:2667-8209

CONTENTS

doi:10.55385/kastamonujes.1424276 KUJES 10(1):1-6, 2024

Kastamonu University
Journal of Engineering and Sciences
e-ISSN 2667-8209
http://dergipark.gov.tr/kastamonujes

Determination of Biological Activity of Some Macro/Micro Algae

Burhan Ceylan[a, *], **Göksal Sezen**[b]

[a] Department of Pharmacognosy, Faculty of Pharmacy, Harran University, Şanlıurfa, Türkiye
[b] Department of Biology, Faculty of Arts and Sciences, Harran University, Şanlıurfa, Türkiye
***Corresponding Author:** b.ceylan022@gmail.com

Received: **January 23, 2024** ◆ Accepted: **June 8, 2024** ◆ Published Online: **June 28, 2024**

Abstract: Algae are primary producers in the aquatic environment and from an important part of the food chain. Algae have secondary metabolites with high biological activity, which are especially important in the creation of novel pharmaceutical agents. Main purpose of the research was to ascertain antioxidant, anti-alzheimer, anti-diabetic and tyrosinase inhibitory activities of ethanol, hexane and water extracts of some macro/micro algae. Maceration was used as the sample prepatation method. Antioxidant activity of algea for different radical and compound was assessed. Anti-Alzheimer activity of the obtained calluses were determined using Ellman method which is a spectrophotometric method. Anti-diabetic activities were determined using the α-glucosidase inhibition method. It was discovered that the water extract contained more antioxidant phytochemicals, including phenolic (587.54±2.12 mg PEs/g DW) and flavonoids (618.39±2.47 mg QEs/g DW). This study confirmed that the water extract contained high levels of biological acitivty. This extract may be utilized as a possible source of beneficial nutrients or antioxidants.

Keywords: Macro/micro algae, antioxidant activity, anti-alzheimer activity, anti-diabetic activity

Öz: Algler su ortamındaki birincil üreticilerdir ve besin zincirinin önemli bir parçasıdır. Algler, özellikle yeni farmasötik ajanların geliştirilmesinde önemli olan, yüksek biyolojik aktiviteye sahip ikincil metabolitlere sahiptir. Bu çalışmada bazı makro/mikro alglerin etanol, hekzan ve su ekstraktlarının antioksidan, anti-alzheimer, anti-diyabetik ve tirozinaz inhibitör aktivitelerinin belirlenmesi amaçlandı. Numune hazırlama yöntemi olarak maserasyon kullanıldı. Farklı radikal ve bileşikler için alglerin antioksidan aktivitesi değerlendirildi. Elde edilen ekstraktların anti-alzheimer aktivitesi spektrofotometrik bir yöntem olan Ellman yöntemi kullanılarak belirlendi. Anti-diyabetik aktiviteler α-glukozidaz inhibisyon yöntemi kullanılarak belirlendi. Su ekstrelerinin fenolik (587.54±2.12 mg PEs/g DW) ve flavonoidler (618.39±2.47 mg QEs/g DW) gibi antioksidan fitokimyasallar açısından daha zengin olduğu bulundu. Bu çalışma, su ekstraktının yüksek düzeyde biyolojik aktivite içerdiğini doğruladı. Bu ekstrakt potansiyel bir antioksidan veya fonksiyonel besin kaynağı olarak kullanılabilir.

Anahtar Kelimeler: Makro/mikro algler, antioksidan aktivite, anti-alzheimer aktivite, anti,diyabetik aktivite

1. Introduction

Algae, one the most important living resources of the seas, ise used in food, agriculture, cosmetics, medicine, pharmacy and industry. Algae have secondary metabolites with high biological activity, which are especially important in the development of new pharmaceutical agents [1]. It is usually found in oceans, rivers, freshwater lakes, streams, arctic lakes, puddles, etc. Algae, which can live in a wide range of aquatic and semi-aquatic environments, are autotrophic and photosynthetic organism. In the food chain, algae play a major role as producers. Algae are becoming more popular since they are used as food in island countries and the Far East. Studies show that seaweed has high nutritional value [2]. Humans have been eating seaweed for thousands of years, and the global market currently stands at over $6 billion annually, with an estimated 12 million tons of seaweed produced in 2018. Coastal habitats are home to a wide range of macroalgea, which are rich sources of bioactive metabolites with diverse biological activities that can affect the survival, dispersion, and abundance of marine species. Based on their color, Seaweeds are categorized into three main categories: Rhodophyta (red algae), Ochrophyta (brown algae), and Chlorophyta (green algae). It is predicted that the maritime environment has 1800 green macroalgae, approximately 1800 brown macroalgae, and 6200 red macroalgae [3].

Antioxidants are frequently introduced into food as food additives to guard against free radicals' oxidative degradation of food. Several naturally occurring compounds found in plants have gained significant interest as safe antioxidants due to their long-standing use by both humans and animals. Thus, it is desirable to create and use more potent antioxidants derived from natural sources [4]. Alzheimer's disease is defined as the knotting of neurofibrils and the formation of amyloids connected to cholinergic neuron loss in regions of the brain related to learning and memory. Acetylcholine level decreases in Alzheimer's patients. One of the ways to treat this is by inhibition of the enzyme responsible fort he hydrolysis of acetylcholine (acetylcholinesterase) [5].

Diabetes mellitus is a comlex illness that can cause serious complications. As a result, the treatment incorporates a variety of therapeutic modalities. Following a meal, postprandial hyperglycemia in diabetes people happens as a result of the gastrointestinal system absorbing glucose. Reducing blood glucose levels in postprandial hyperglycemia, a common condition among diabetics, can be achieved by inhibiting intestinal glucose absorption and promoting tissue glucose absorption [6]. The purpose of this investigation was to ascertain the antioxidant, anti-alzheimer, anti-diabetic and tyrosinase inhibitory activities of ethanol, hexane and water extracts of some macro/micro algae (*Dunaliella salina*, *Microcystis aeroginosa*, *Myriophyllum spicatum*, *Chrolella vulgaris*, *Aphanizomenon flasaque*, *Spiruline palatensis* and *Cladophora glomerata*)..

2. Material and Method

Chemicals and spectral measurements

Acetylcholinesterase (AChE) and butyrylcholinesterase (BChE), 5,5'-dithiobis (2-nitrobenzoic) acid (DTNB), acetylthiocholine iodide (AcI) and butyrylthiocholine chloride (BuCl), phosphate buffer (pH 6.8-8.0), galantamine, p-nitrophenyl-α-D-glucopyranoside (p-NPG), genistein, linoleic acid, α-tocopherol, potassium persulfate, nicotinamide adenine dinucleotide (NADH), butylated hydroxyanisole (BHA), butylated hydroxytoluene (BHT), nitroblue tetrazolium (NBT), phenazine methosulfate (PMS), 1,1-diphenyl-2-picrylhyrazyl (DPPH), pyrocatechol, quercetin and 3-(-pyridyl)-5,6-bis(4-phenyl-sulfonic acid)-1,2,4-triazine (ferrozine) were obtained from Sigma Chemical Co. (Sigma-Aldrich GmbH, Sternheim, Germany). α-glucosidase, dimethyl sulfoxide (DMSO), methanol, ethanol were purchased from Merck (Darmstadt, Germany). The BioTek Power Wave XS (USA) 96-well microplate was used for the bioactivity measurements. Utilizing Gen5 Data Analysis software, the measurements and computations of the activity data were assessed. Ammonium thiocyanate, ferrous chloride, polyoxyethylenesorbitan monolaurate (Tween-20), tricholoroacetic acid (TCA), ethanol (EtOH) and hexane were acquired from Merck. The remaining substances were acquired through Sigma-Aldrich or Merck and were all of analytical quality. Water was puridifed by Human (Japan) ultrawater purification system.

Materials and extraction procedures

Dunaliella salina, *Chrolella vulgaris* and *Spirulina platensis* were obtained from Çukurova University, Faculty Aquaculture. *Cladophora glomerata*, *Microcystis aeroginosa* from Sanlıurfa Birecik Karkamış Dam; *Aphonizomenon flasaque* and *Myriophyllum spicatum* from Sanlıurfa Siverek Çamçayı Dam. collected by Göksal Sezen. The collected algae were cleaned of stones, sand and invertebrates (mussels and snails), dried in the shade, pulverized with a 46000 rpm blender (Tefal Ultra High Speed Blender) and stored in the deep freezer at -20 ºC. Algae were placed in 20 liter plastic bottles in the Hydrobiology-Algology laboratory of the Biology Department of the Faculty of Science and Letters, Harran University. Preparation of the extracts was done according to the method we developed in our previous study [4]. To prepare the water extract, 25 g algae sample and 500 mL of boiling water were mixed in a magnetic stirrer for quarter of an hour. The extract was then filtered and evaporated to dryness in a rotary evaporator under lower pressure and controlled temperature (40-50 ºC). To prepare ethanol and hexane extracts, 25 g algae sample was mixed with 500 mL of solvent. Then, it was incubated for 3 hours in a shaking water bath at 100-150 rpm at room temperature (25 ºC). The residue was re-extracts until extraction solvents are colerless Using filter paper, the extracted materials were purified (Whatman No.1 paper) and the solvents of the filrates (ethanol and hexane) were evaporated in a rotary evaporator (Buchi R-200, Switzerland) at 40-80 ºC. Following the creation of the water extracts, the filtrate was lyophilized after being filtered via filter paper (at 5 µm Hg pressure at – 50 ºC [Labconco, Freezone 1 L]). Before being used, each extract was dissolved in solvent or water and stored at -20 ºC.

Total phenolic and flavonoid contents

The analysis of the specimens revealed that the overall phenolic [7] and flavonoid [8] contents were comparable to quercetin and pyrocatechol, respectively. For fermented non-alcoholic drinks, the overall levels of phenolic and flavonoid compounds were determined using the following formulae.

Absorbance = 0.001x - 0.0012 pyrocatechol (µg) (r^2 = 0.9978)

Absorbance = 0.0007x + 0.0012 quercetin (µg) (r^2 = 0.9983)

Antioxidant activity

The β-carotene/linoleic acid bleaching assay, ABTS cation radical scavenging, DPPH free radical scavenging assays, superoxide anion radical scavenging, hydrogen peroxide scavenging activity, and CUPRAC (Cupric reducing antioxidant capacity) assay were a total of six methods were employed to evaluate the specimen's antioxidant activity (4). To

determine the samples' IC50 (50% inhibition), doses of 100, 50, 25, and 10 µg/mL were generated. As standards, BHA, BHT, and α-tocopherol were employed in these six antioxidant test techniques.

Anticholinesterase activity

The spectrophotometric technique created by Ellman et al [9] was slightly modified to evaluate the inhibitory activities of acetyl- and butyryl-cholinesterase. The reaction's substrates were acetylthiocholine iodide and butyrylthiocholine iodide, and DTNB was employed to gauge the anticholinesterase activity. Methanol was used to dissolve each callus culture in order to create stock solutions at a concentration of 4000 g/mL. The following ingredients were combined and incubated for 15 minutes at 25 ºC: 150 microliters of 100 mM sodium phosphate buffer (pH 8.0), 10 g/mL of sample solution, 20 l of AChE (or BChE) enzyme solution, and 10 g/mL of DTNB. Acetylthiocholine iodide (or butyrylthiocholine iodide) 10 g/mL was then added to start the reaction. The callus culture's final concentration in solution was 10, 25, 50, and 100 g/mL. The production of yellow 5-thio-2-nitrobenzoate anion with a wavelength of 412 nm, which occurs when DTNB reacts with thiocholine produced by the enzymatic hydrolysis of acetylthiocholine iodide or butyrylthiocholine iodide, served as a marker for the hydrolysis of these substrates. The samples and controls were dissolved in methanol, which served as a solvent. Galantamine was used as standard.

α-glucosidase inhibitory activity

The callus culture was evaluated for the inhibition of Saccharomyces cerevisiae's -glucosidase using a technique somewhat modified by Tsujii et al [10]. In a nutshell, a 40 L solution of -glucosidase (3.0 U/mL, dissolved in phosphate buffer, pH 6.8) was pre-incubated at 37 ºC for 30 min with 10 L of each callus culture in DMSO. P-nitrophenyl-D-glucopyranoside (p-NPG; final concentration 0.5 mM) was added to the mixture to start the enzymatic reaction, which continued for another 30 minutes. Observing the p-nitrophenol produced from p-NPG at 405 nm allowed researchers to ascertain the -glucosidase activity. The positive control utilized was genistein.

Statistical analysis

A power analysis was done to figure out how many extracts of algae there were. The findings were shown as means ± standard deviation as n=3 for each test specimen.

3. Result

Extraction yield, total phenolic and flavonoid contents

The percentage yields of algae extracts displayed in Table 1. The highest extraction efficiency was seen in water extracts and the percent extraction yields of the water extracts varied between 66.44% and 60.10%. The percent extraction yields of the ethanol extracts varied between 42.66% and 38.93%. The percent extraction yields of the hexane extracts varied between 22.90% and 18.66%. Therefore, all of the extractable components were greater in the water extract. Food secondary metabolites known as phenols or polyphenols are significant because of their antioxidant activity, which involves chelating redox-active metal ions, initiating lipid free radical chains, and blocking the process of transformation of hydroperoxide into reactive oxygen radicals. The total phenolic content of the ethanol extracts differentiating between 407.44±1.38 and 420.47±1.66 µg PEs/mg extract. The extract from *Myriophyllum spicatum* has the greatest total phenolic content among the ethanol extracts (163.61±0.94 µg PEs/mg extract). Total flavonoid content od hexane extracts ranged from 368.60±0.72 to 382.66±0.82 µg QEs/mg extract. The highest total flavonoid content of hexane extracts was detected in *Myriophyllum spicatum* extract (382.66±0.82 µg QEs/mg extract). These quantities were similar to the outcomes for the other algae product extracts reported in the available research. Keramane et al [11] in their study found the extraction efficiency of *Padina pavonica* (Brown algae) to be 4.25% and the total phenolic content to and 49.82±1.40 mg GAE/g extract [11]. Since The water extract had the most extraction efficiency, as shown, this extract was used in antioxidant, anti-Alzheimer and anti-diabetic acitivity determinations.

Table 1. Extraction yields and contents of total phenols, total flavonoids in algae extracts

Algae samples	Extraction solvent	Extraction yield (%)	Total phenolic content (µg PEs/mg extract)[a]	Total flavonoid content (µg QEs/mg extract)[b]
Dunaliella salina	Hexane	22.53	345.84±0.94	380.98±0.61
	Ethanol	41.16	418.77±1.25	472.59±1.51
	Water	66.44	587.54±2.12	618.39±2.47
Chrolella vulgaris	Hexane	20.08	340.24±0.78	371.24±0.83
	Ethanol	38.93	407.44±1.38	463.80±1.56
	Water	62.75	579.81±2.17	614.75±2.33
Spirulina platensis	Hexane	18.66	339.79±0.77	365.32±1.99
	Ethanol	42.40	415.63±1.82	473.11±2.80
	Water	60.10	570.39±2.43	600.67±2.65

	Hexane	21.85	341.35±0.71	375.63±0.58
Cladophora glomerata	Ethanol	40.38	410.94±1.58	466.40±1.64
	Water	64.10	581.77±2.40	616.82±2.80
	Hexane	19.37	343.26±0.79	368.60±0.72
Microcystis areroginosa	Ethanol	41.93	416.02±1.74	296.33±1.70
	Water	65.75	584.14±2.87	617.52±2.31
	Hexane	20.66	342.60±0.63	372.69±0.74
Aphonizomenon flasaque	Ethanol	40.90	411.88±1.45	468.23±1.59
	Water	63.18	583.61±2.33	612.60±2.70
	Hexane	22.90	347.58±0.84	382.66±0.82
Myriophyllum spicatum	Ethanol	42.66	420.47±1.66	475.18±1.60
	Water	61.34	572.50±2.22	607.42±2.88

[a]*Phenolic content equivalent to pyrocatechol ($y=0.001x-0.0012$ $R^2=0.9978$)*
[b]*Flavonoid content equivalent to quercetin ($y=0.0007x+0.0012$ $R^2=0.9983$)*

Antioxidant activity

The antioxidant activity of algae was tested by the β-carotene/linoleic acid bleaching assay, ABTS cation radical scavenging, DPPH free radical scavenging assays, superoxide anion radical scavenging, hydrogen peroxide scavenging activity, CUPRAC (Cupric reducing antioxidant capacity) assay for reducing antioxidant activty. The antioxidant activity test results are given in Table 2. In DPPH• radical scavenging activity, all algae water extracts exhibited higher (stronger) antioxidant activity than standards (except *Cladophora glomerata*). Among all algae, *Cladophora glomerata* exhibited the lowest antioxidant activity.

Table 2. IC_{50} values(μg/mL) of DPPH• free radical scavenging activity, ABTS•+ cation radical scavenging activity, hydrogen peroxide scavenging activity and superoxide anion scavenging activity of algae water extracts (100 μg/mL)

Extracts and standards	**Scavenging ability on DPPH• free radicals**	**Scavenging ability on $ABTS^{\bullet+}$ cation radicals**	**Scavenging ability on hydrogen peroxide**	**Scavenging ability on superoxide anion**	**CUPRAC assay**
Dunaliella salina	57.14±1.32	35.22±0.13	41.26±1.46	63.85±2.59	21.28±1.03
Chrolella vulgaris	43.27±1.33	36.40±0.55	40.81±1.33	65.48±2.29	20.93±1.14
Spirulina platensis	50.28±2.11	38.23±0.62	42.38±1.77	67.50±2.30	19.85±0.97
Cladophora glomerata	36.15±0.49	33.17±1.05	38.40±1.18	60.47±2.83	12.53±0.81
Microcystis aeroginosa	54.35±1.48	34.38±1.30	44.61±0.71	64.93±2.08	18.87±0.91
Aphanizomenon flasaque	48.63±1.22	35.96±0.78	41.90±0.96	62.66±2.61	20.34±1.20
Myriophyllum spicatum	44.75±0.95	36.05±1.11	43.26±0.58	63.01±2.18	19.08±0.63
BHA	40.80±1.73	28.67±0.49	37.62±1.30	57.14±2.23	10.85±0.60
BHT	40.28±1.45	30.23±0.52	36.40±0.83	58.63±2.40	11.02±0.20
α-tocopherol	39.53±1.19	32.81±0.85	35.30±0.44	55.50±2.33	10.39±0.12

Values are given as the mean and standard deviation of three parallel measurements.

Anti-alzheimer activity

Acetylthiocholine iodide is utilized as the substrate and acetylcholinesterase enzyme is employed as the inhibitor of acetylcholinesterase activity. The reaction is based on the formation of the yellow 5-thio-2-nitrobenzoate anion with DTNB of the thiocholine formed as a result of the acetylcholine iodide decomposition by the acetylcholinesterase enzyme and its spectrophotometric measurement at 412 nm. The standard is galantamine, an isolated alkaloid substance from the Galanthus plant. Ethanol was used as a control. Anticholinesterase activity was determined as % inhibiton relative to control using the following equation.

% inhibition = (Acontrol – Asample / Acontrol) × 100

Acontrol = Ethanol absorption

Asample = Algae water extracts

Algae extracts showed anti-Alzheimer activity in direct proportion to the increase in concentration. According to table 3, although galantamine was used as a standard, it did not show 100% inhibition. Therefore, assuming 100% inhibition of

galantamine, algae water extracts showed moderate anti-alzheimer's activity relative to galantamine. Among all algae, *Cladophora glomerata* exhibited the lowest anti-Alzheimer activity in Table 3.

Table 3. Anticholinesterase inhibition of algae extracts and standard

Algae Samples (water extracts)	**% inhibition of acetylcholinesteras**
Dunaliella salina	57.14±1.20
Chrolella vulgaris	53.27±1.30
Spirulina platensis	52.18±1.11
Cladophora glomerata	41.45±1.49
Microcystis aeroginosa	53.35±1.28
Aphanizomenon flasaque	54.80±1.53
Myriophyllum spicatum	52.28±1.75
Galantamine	80.53±1.49

Anti-diabetic activity

A class of medications used to treat diabetes prevents the conversion of carbohydrates into glucose by blocking the enzymes -amylase and -glucosidase, which are included in the analysis of carbohydrates in metabolism. Extracted callus tissue cultures were made according to the method described for inhibition of α-glucosidase from Saccharomyces cerevisiae. Genistein was used as a standard. The control group was analyzed by changing samples with phosphate buffer. α-glucosidase inhibition activity was calculated as % inhibiton relative to control using formulation below.

% inhibition = (Acontrol – Asample / Acontrol) × 100

Acontrol = Phosphate buffer

Asample = Callus culture extracts

Algae extracts showed anti-diabetic activity in direct proportion to the increase in concentration. According to table 4, although genistein was used as a standard, it did not show 100% inhibition. Therefore, assuming 100% inhibition of genistein, algae water extracts showed moderate anti-alzheimer's activity relative to genistein. *Dunaliella salina* exhibited the highest anti-diabetic activity among algae samples in Table 4.

Table 4. α-glucosidase inhibition of algae extracts and standard

Algae Samples (water extracts)	**% inhibition of α-glucosidase**
Dunaliella salina	66.64±2.70
Chrolella vulgaris	63.07±2.33
Spirulina platensis	62.28±2.51
Cladophora glomerata	51.25±2.20
Microcystis aeroginosa	63.75±2.48
Aphanizomenon flasaque	61.20±2.23
Myriophyllum spicatum	60.14±2.35
Genistein	88.63±2.09

4. Discussion and conclusion

The results of this research reveal the early details on the anticholinesterase, antidiabetic, and antioxidant properties of algal extracts. The aqueous extract of the algae sample (*Spirulina platensis*) showed the highest effectiveness among the three evaluated techniques for inhibiting scavenging ability on superoxide anion. The aqueous extracts had much more DPPH-scavenging activity than the benchmarks BHA, BHT, and α-tocopherol. As is well known, phenolic content and free radical-scavenging activity—particularly with regard to the DPPH radical—have a strong linear relationship. The water extracts also showed strong scavenging ability on ABTS cation radicals. The water extract showed results close to the standards (galantamine and genistein) in anti-Alzheimer and anti-diabetic activity. Zaid et al [12] found the total phenolic substance content of *Spirulina platensis* extract to be 40 mg/g [12]. Trigui et al [13] found the acetyl choline esterase activity of ethyl acetate extract of *Ulva rigida* to be 7.6 mg/mL [13]. Therefore, the algae may shield humans from the damaging effects of free radicals and lipid peroxidation, and its extracts are likely be useful in the creation of

safe food additives and goods. This algae's ability to scavenge free radicals could represent one of the ways that it serves both a culinary and traditional medicinal purpose. It is necessary to conduct more research on specific molecules (secondary metabolites), their biological actions in vivo, and various biological pathways. The usage of algal water extracts as a natural source of antioxidants was determined.

Conflict of Interest

All authors certify that they have no affiliations with or involvement in any organization or entity with any financial interest or non-financial interest in the subject matter or materials discussed in this manuscript.

Ethics Committee Approval

Ethics committee approval is not required.

Author Contribution

Conceptization: BC, GS; methodology and laboratory analyzes: BC, GS; writing draft: BC, GS; proof reading and editing: Other: All authors have read and agreed to the published version of manuscript.

Acknowledgements

Not appliable

5. References

[1] Chapman, R.L., Buchheim, M.A. (2001). Green algae and the evolution of land plants: inferences from nuclear-encoded rRNA gene sequences. Biosystems. 28(1-3): 127-137.

[2] Barbier, P., Guise, S., Huitorel, P., Amade, P., Pesando, D., Briand, C., Peyrot, V. (1992). Caulerpenyne from Caulerpa taxifolia has an antiproliferative activity on tumor cell line SK-N-SH and modifies the microtubule network. Life science. 70(4): 415-429

[3] Belton, G.S., Draisma, S., Van Reine, W.F.P., Huisman, J.M., Gurgel, C.F.D. (2019). A taxonomic reassessment of Caulerpa (Chlorophyta, Caulerpaceae) in southern Australia, based on tufA and rbcL sequence data. Pyhcologica. 58(3): 234-253

[4] Ceylan B., Yeşiloğlu, Y. (2022). Investigation of antioxidant activity of Sorbus domestica L. extracts and determination of phenolic contents by LC-MS/MS. Revue Roumaine de Chimie. 67(6-7): 343-351

[5] Ertaş, A., Gören, A.C., Boğa, M., Yeşil, Y., Kolak, U. (2014). Essential oil compositions and anticholinesterase activities of two edible plants Tragopogon latifolius var. angustifolius and Lycopsis orientalis. Natural Product Research. 28(17): 1405-1408

[6] Thilagam, E., Parimaladevi, B., Kumarappan, C., Mandal, S.C. (2013). α-glucosidase and α-amylase inhibitory activity of Senna surattensis. Journal of Acupuncture and Meridian Studies. 6(1): 24-30

[7] Moreno, M.I.N., Isla, M.I., Sampietro, A.R., Vattuone, M.A. (2000). Comparasion of the free radical-scavenging activity of propolis from several regions of Argentina. Journal of Ethnopharmacology. 71(1-2): 109-114

[8] Slinkard, K., Singleton V. (1977). Total Phenol Analysis: Automation and Comparasion with Manual Methods. American Journal of Enology and Viticulture. 28: 49-55.

[9] Ellman, G.L., Courtney, K.D., Andress, V.J., Feather-Stone, R.M. (1961). A new rapid colorimetric determination of acetylcholinesterase activity. Biochemistry Pharmacology. 7: 88-95

[10] Tsujii, E., Muroi, M., Shiragami, N., Takatsuki, A. (1996). Nectrisine is a potent inhibitor of alpha-glucosidases, demonstrating activities similarly at enzyme and cellular levels. Biochemical and Biophysical Research Communications. 220(2): 459-466

[11] Keramane, B., Sanchez-Camargo, A.P., Montero, L., Laincer, F., Bedjou, F., Ibanez, E. (2023). Pressurized liquid extraction of bioactive extracts with antioxidant and antibacterial activity from green, red and Brown Algerian algae. Algal Research 76: 103293.12. Ellman GL, Courtney KD, Andress VJ, Feather-Stone RM. A new and rapid colorimetric determination of acetylcholinesterase activity, Biochem. Pharmacology. 7: 88-95

[12] Zaid, A. A. A., Hammad, D. M., & Sharaf, E. M. (2015). Antioxidant and anticancer activity of Spirulina platensis water extracts, 11(7): 846-851.

[13] Trigui M., Gasmi L., Zouari I., Tounsi S. (2013). Seasonal variation in phenolic composition, antibacterial and antioxidant activities of *Ulva rigida* (Chlorophyta) and assessment of antiacetylcholinesterase potential. J. Appl. Phycol. 25: 319-328.

doi:10.55385/kastamonujes.1449504 KUJES 10(1):7-14, 2024

Kastamonu University
Journal of Engineering and Sciences
e-ISSN 2667-8209
http://dergipark.gov.tr/kastamonujes

Effect of Mechanical Alloying Time on Microstructure, Hardness and Electrical Conductivity Properties of Cu-B_4C Composites

Hasaneen Houssain[a, b*], Ahmet Oğuzhan Cengiz[c], Serkan Islak[c]

[a]Institute of Science, Kastamonu University, Kastamonu, Türkiye
[b]Department of Chemical Engineering, Faculty of Engineering, Al Muthanna University, Samawah, Iraq
[c]Department of Mechanical Engineering, Faculty of Engineering and Architecture, Kastamonu University, Kastamonu, Türkiye
***Corresponding Author:** hasanein.mahbuba@gmail.com

Received: **March 9, 2024** ◆ Accepted: **May 22, 2024** ◆ Published Online: **June 28, 2024**

Abstract: This study aims to investigate the effect of mechanical alloying time on the microstructure, hardness, and electrical conductivity properties of copper (Cu) matrix boron carbide (B_4C) reinforced composites. Cu-B_4C composites with 2% B_4C by volume were subjected to mechanical alloying processes for 0, 1, 5, 10, and 20 hours. The microstructure and phase formation of the composites were examined using scanning electron microscopy (SEM) and X-ray diffraction (XRD). Hardness measurements of the composites were conducted using the microhardness measurement method, and density values were determined using the Archimedes principle. The electrical conductivity values of the samples were measured in terms of the international annealed copper standard (%IACS) based on the eddy current principle. SEM images revealed a more homogeneous distribution of B_4C particles in the Cu matrix as the mechanical alloying time increased. Hardness values showed significant increases with the increasing mechanical alloying time, reaching the highest value in the 20 h milled sample with a 90.86 value. The effect on electrical conductivity values was noteworthy, with a measurement of 63% IACS at 0 hours and 25% IACS at 20 hours of mechanical alloying.

Keywords: Cu-B_4C composites, mechanical alloying time, electrical conductivity, microstructure, hardness

Öz: Bu çalışma mekanik alaşımlama süresinin bakır (Cu) matrisli bor karbür (B_4C) takviyeli kompozitlerin mikroyapı, sertlik ve elektriksel iletkenlik özelliklerine etkisinin araştırılmasını amaçlamaktadır. Hacimce %2 B_4C ilave edilen Cu-B_4C kompozitler 0, 1, 5, 10 ve 20 saat mekanik alaşımlama işlemine tabi tabi tutulmuştur. Kompozitlerin mikroyapı ve faz oluşumu taramalı elektron mikroskobu (SEM) ve X-ışınları difraktometresi (XRD) ile incelenmiştir. Kompozitlerin sertlik ölçümleri mikrosertlik ölçüm yöntemi ile yoğunluk değerleri ise Arşiment prensibi ile ölçümü gerçekleştirilmiştir. Numunelerin elektriksel iletkenlik değerleri girdap akım prensibine göre uluslararası tavlanmış bakır standardı (%IACS) cinsinden ölçülmüştür. SEM görüntüleri mekanik alaşımlama süresi arttıkça B_4C tanelerinin Cu matrisinde daha homojen dağıldığını göstermiştir. Sertlik değerlerinde ise mekanik alaşımlama süresinin artmasıyla belirgin artışlar olmuş olup, en yüksek değer 20 saatlik numunesinde 90.86 değeri ile olmuştur. Elektriksel iletkenlik değerleri üzerine ise mekanik alaşımlama süresinin kayda değer seviye olmuştur. 0 saat değerinde %63 IACS iken, 20 saat mekanik alaşımlama değerinde ise %25 IACS ölçülmüştür.

Anahtar Kelimeler: Cu-B_4C kompozitler, mekanik alaşımlama süresi, elektriksel iletkenlik, mikroyapı, sertlik

1. Introduction

Metal matrix composites (MMCs) are a type of material that combines a continuous metallic matrix with a reinforcement, typically made of ceramic. The matrix can be made of various metals and their alloys, including aluminum, titanium, copper, nickel, and magnesium. The ceramic reinforcement is usually made of materials such as oxide, carbide, nitride, or borides [1-3]. Copper and its alloys are widely used in industrial applications, especially in areas where conductivity plays a significant role due to their unique combination of excellent thermal and electrical properties, low cost, ease of manufacturing, and good corrosion resistance [4, 5]. Nevertheless, pure copper has some significant drawbacks, such as low strength, high coefficient of thermal expansion (CTE), and generally poor mechanical properties. One of the most effective ways to address these limitations is to reinforce copper with ceramic particles to create composites with superior properties without causing any weakening of both thermal and electrical conductivities of copper [6]. Much research produced MMCs with developed properties, such as designing Cu-based alloys reinforced with ceramics. Fathy and El-Kady [6] used powder metallurgy (P/M) technology to fabricate copper-alumina composites and successfully controlled the thermal properties of the produced copper alloy. Shaik and Golla [7] prepared Cu–ZrB_2 composite to improve copper mechanical properties and control its thermal features, they conducted their investigation utilizing the ball milling technique for 20h and consolidating the mixed powder by the hot-pressing method. Understandably, the properties of MMC are affected by milling conditions like milling time, rotating speed, milling environment, etc., however, many

researchers studied the influence of milling time on the microstructure, as well as, the forming of the phases of Cu matrix-based alloys [8, 9]. Nevertheless, the effect of milling time on the properties of Cu matrix alloys is still not fully studied. Therefore, in this research, Cu-B_4C matrix composite alloys were prepared and the effect of milling times on microstructure as well as physical and mechanical properties were investigated.

2. Material and Method

In this work, 98% Cu and 2% B_4C powders with a purity of more than 95% and 325 mesh were utilized for fabricating Cu-B_4C composite alloy, the raw powders were supported from Nanografi Nanotechnology Company, as received powders mixed using mechanical mixing for variant mixing times while the other milling conditions remained constant to investigate the effect of mixing durations on produced alloys properties, the process parameters are given in Table 1. Then gained mixed powders were cold pressed into a cylindrical mold of 20 mm in diameter and 5 mm in thickness using a hydraulic press device at 700 MPa pressing load. Then the green alloys underwent a sintering process for 60 minutes at 850 ºC utilizing a tubular furnace with argon gas atmosphere. The schematic of alloys fabricating process illustrates in Figure 1.

Table 1. Powder composition and process parameters

Sample group	Compositions (vol.%)		Mechanical alloying time (Hour)	Sintering Temperature (ºC)	Sintering Time (Minutes)
	Cu	B_4C			
CB0	98	2	0	850	60
CB1	98	2	1		
CB5	98	2	5		
CB10	98	2	10		
CB20	98	2	20		

The samples were prepared by abrasion and polishing process using 320-1500 grade sandpaper and polished using 1um of diamond solution. The etching process was achieved using Kroll etchant to conduct a microstructure investigation test. Microstructure examination and phase analysis were achieved utilizing the scanning electron microscope brand FEI QUANTA 250 FEG and X-ray diffraction (Bruker D8 Advance). The experimental densities of the samples were calculated depending on Archimedes principal meeting with ASTM B 962 [10]. The hardness of the samples was evaluated using the Shimadzu HMV G21 model microhardness device according to the ASTM E92-17 standard ("Standard Test Methods for Vickers Hardness and Knoop Hardness of Metallic Materials," 2017). The hardness load was 2 Kg, and 15 seconds of holding time. Furthermore, to study the effect of B_4C and Mixing duration on electrical properties, the electrical conductivity test was conducted by a Nortec 500 D device utilizing the Eddy current principle according to TS EN ISO 15549 standards.

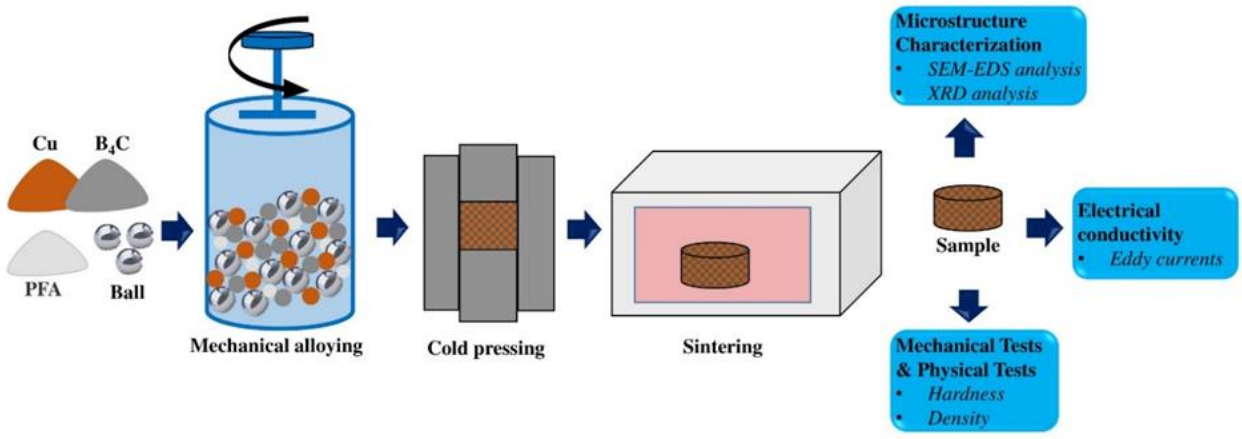

Figure 1. Flow chart of production and applied testing and analysis

3. Result and Discussions

Figure 2 shows the XRD patterns of Cu-B_4C alloys ball milled for 0, 5, and 20 hours. The patterns indicated the existence of the Cu phase only, which can be attributed to the low B_4C content of 2 % in the Cu Matrix. Shik et al. [7] in their work, related the appearance of just the Cu phase in XRD pattern due to low content of ZrB_2 up to 5%. Hamid et al [5] in their study, indicated existing only Cu peaks in the XRD pattern of Cu sample containing 3% wt. of TiC and Al_2O_3; they

attributed that to the small amount utilized of both TiC and Al_2O_3. More significantly, as can be seen in (Figure 2), the XRD patterns of the samples milled for variant times showed more sharpness intense, and narrow peaks as the milling time increased which confirmed the finer grain size and more crystallinity. The study of the grain size and investigation of the effect of milling time on particle size is essential in understanding the properties of the Cu–B_4C alloys. The broadening of XRD peaks was employed to estimate the particle size using Debye-Scherrer (Equation 1). The following formula was performed [11]:

$$\boldsymbol{D = \frac{0.9\,\lambda}{\beta \cos \theta}} \qquad \text{Eq (1)}$$

Where D is the particle size, β is the full width at half maximum height, θ is the peak Bragg's angle, λ is the X-ray wavelength.

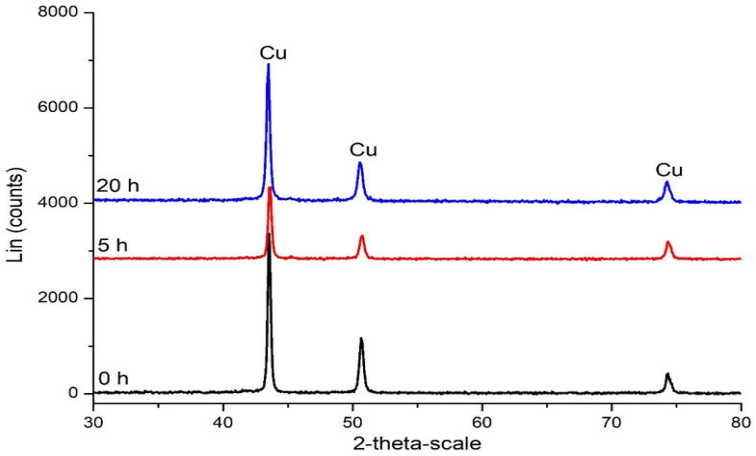

Figure 2. XRD pattern of Cu-B_4C milled for 0, 5, and 20 hours

Figure 3 illustrates the influence of the milling time on the crystallite size. A clear decrease in the crystallite size can be observed with a longer milling time, where the particle size of the alloy produced without mechanical mixing was 36.79 nm, while the alloy milled for 5 hours had a reduction in particle size to 33.37 nm. Furthermore, the crystalline size was reduced to 32.87 nm for the alloy that was milled for 20 hours. This reduction in particle size with longer milling time can be attributed to various factors such as dominant fracture mechanism, severe work hardening, and collisions between the ball-to-wall, ball-to-ball, and powder-to-powder; these factors result in the fracturing of the powder particles into smaller particles and as a result a smaller crystal size of alloy [12]. These outcomes met with other literature; in their work, Liu et al. [13] achieved a smaller particle size of Al composite alloy with a prolonged mixing time of up to 10 hours. In their research, Salur et al. [12] recorded that the average crystallite size decreased as milling time increased.

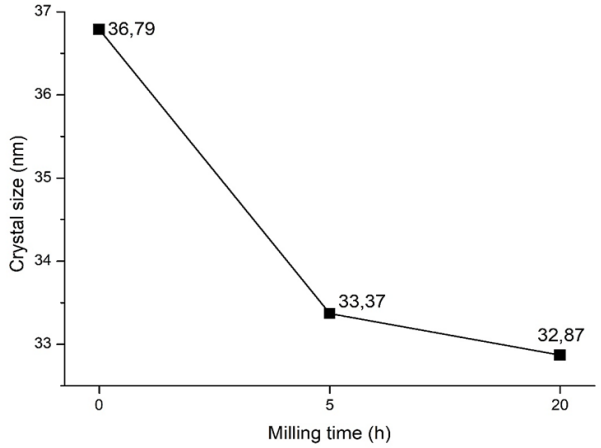

Figure 3. Effect of milling time on crystal size

Figure 4 shows the SEM images of Cu-B_4C sampled milled for 0, 1, 5, 10, and 20 hours. The size and shape of particle and crystal structure of alloys that are processed by the mechanical alloying approach are extremely conditional on the processing parameters. The most influential processing parameters are the milling time, milling environment, ball-to-powder ratio, milling speed, and process control agent [11]. It is seeable from the SEM images in (Figure 4a-f) that there is almost no porose occurring in the samples, indicating that a compact structure has been constructed. Moreover, as can be observable from SEM images, the structure of the alloys is a constituent from the Cu matrix grain with particles of

B_4C distributed through the Cu matrix. EDS analysis (Figure 4f) supports the appearance of Cu, B, and C, confirming the formation of the mentioned structure. However, (Figure 4a) represents the initiated sample without milling, the main view of the matrix structure is a long fragment of matrix particle with almost non-uniform shape and size and the B_4C particles diffused through the matrix. As the milling time is conducted for 1 hour (Figure 4b), the alloy matrix structure becomes a flaky-like form and more uniform compared to the initial alloy due to cold welding during milling [7]. As the milling time progresses for 5 hours (Figure 4c) more flattening and uniform can be observed, again, further mechanical welding effects with a longer milling time become evident. the particles of a relatively larger size which flattened after 1 hour of milling, begin to break gradually after 2 hours of milling. These flattened particles further get fragmented and exhibit an asymmetrical behavior, resulting in a decrease in the average particle size [12]. This observation is supported by crystallite size chart (Figure 3). when 10 hours of milling time is achieved, (Figure 4d), the structure of alloys tends to be more homogenous and the grains become considerably smaller in contrast to lower milling time alloys. Again, the further milling time led to more particle fractions and more cold welding which reflected positively in the diffusing of B_4C through the matrix, which is clearly observable from the SEM image (Figure 4d) which shows the more uniformity distributed of B_4C throughout the Cu matrix. Shaik et al [7] achieved a uniform distribution of ZrB_2 in the Cu matrix when achieving a 10 h milling time. Furthermore, when milling time progressed to 20 h, (Figure 4f), the microstructure becomes clearly defined, as can see, the grain and grain boundary are clearly shown without flaky structure, and the structure becomes more compact and the B_4C distributed with further homogenously in Cu matrix as notable from (Figure 4f) of mapping image for elements distribution. This can be described by when the ball milling process exceeds 10 hours and the mixing process reaches 20 hours, it enters into a steady state. In other meaning, there is a dynamic balance between fracture and cold-welding mechanisms, which occurs in the final stage of ball milling, during this stage, the particles within the system experience approximately the same rate of change, leading to the reduction of larger particles and the growth of smaller particles at a similar rate, this action results in the particles becoming roughly equal in shape [8, 14]. This behaver also helps the reinforcement particles to diffused uniformly throughout the matrix [7].

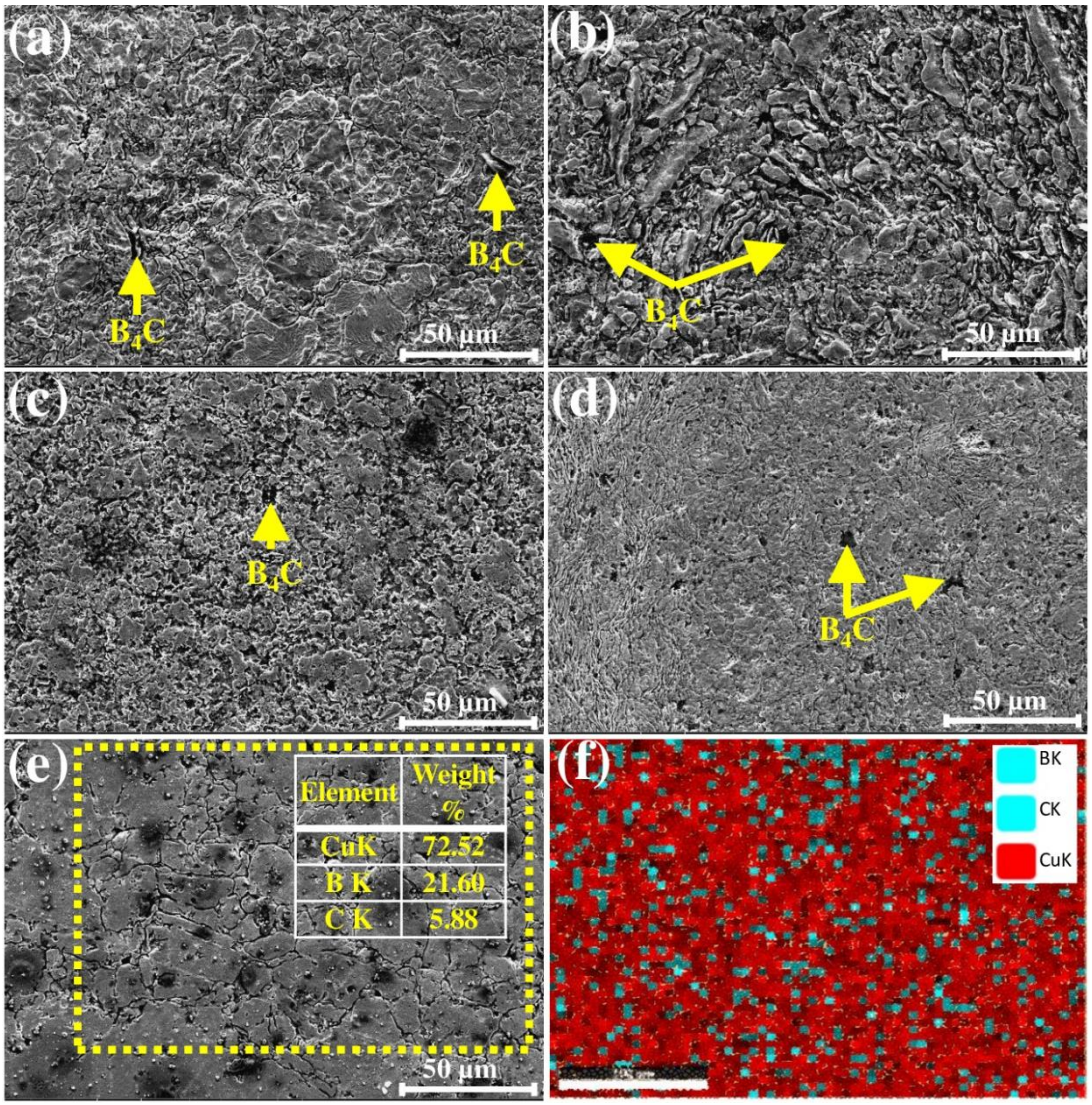

Figure 4. SEM images of samples milled for (a) 0 h, (b) 1 h, (c) 5 h, (d) 10 h, (e) 20 h and EDS analysis, (f) MAP-EDS

Figure 5 illustrates the impact of mixing time on the experimental density, relative density, and porosity of Cu/B_4C composites. As per the graph, both experimental density and relative density reduce, and porosity increases with an increase in mixing time. The experimental densities of alloys mixed for 0, 1, 5, 10, and 20 hours were 7.48, 7.29, 7.04, 6.63, and 6.50 g/cm^3, respectively. Similarly, the relative densities were 84.72%, 82.59%, 79.76%, 75.15%, and 73.63%, respectively. This reduction in density is due to the low density of the B_4C reinforcing element (2.52 g/cm^3) compared to the Cu matrix (8.94 g/cm^3). Zhou and Duszczyk [15] added SiC to Aluminum alloy type AA2014 and fabricated Al/SiC alloy. They reported a decrease in densities when adding SiC. Similarly, Kriewah and Islak [16] reported that reinforcement material with low density compared to the matrix reduces the density of the composite. The decreasing density with increasing mixing duration may related to that the longer mixing time means a more homogenous distribution of ceramic particles through the matrix, moreover, also attributed to B_4C particle fragmentation which restricts the rearrangement of matrix metal powder particles during sintering [17]. The reduction in relative densities is due to two reasons. Firstly, the fact that the ceramic particles added to the metallic matrix negatively affect the sintering ability and prevents the matrix particles from necking. Secondly, related to the difference in melting temperature between the matrix and the reinforcement elements which means more porose in the final alloy microstructure [18]. However, the porosity rates were estimated as 15.27%, 17.4%, 20.23%, 24,84%, and 26.36%, for 0, 1, 5, 10, and 20 hours of mixing duration, respectively. The increase in porosity can be associated with the decrease in relative density.

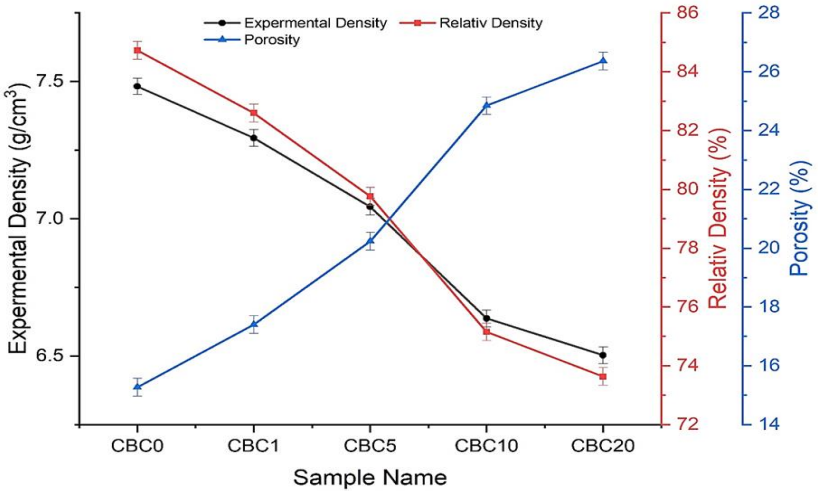

Figure 5. Effect of milling time on Experimental density, relative density, and porosity

Figure 6 shows the effect of mixing duration on hardness values, which is ceramic alloy composites' most important mechanical property. Vickers hardness values of samples mixed for (0, 1, 5, 10, and 20) hours were (56.82, 67.22, 80.58, 87.62, 90.86) respectively. The increase in hardness clearly can be noted as the longer mixing duration. The hardness increase was about 59.9% for the sample mixed for 20 hours compared to a sample without mixing. The increase in hardness with increased milling time attributed to the longer time means more fine powder particles and decreasing in primary grain. Also, more mixing duration leads to a more homogenous distribution of B_4C, and the B_4C may behave as an obstacle to primary grain growth, causing smaller grain as a result [13]. Some researchers attributed that the finer particles mean the greater interfacial area between reinforcement and matrix phases [19]. Moreover, the Hall-Petch (Equation 2) indicated that the hardness is inversely relation to grain size.

$$\boldsymbol{H = H_0 + KD^{-1/2}} \qquad \text{Eq (2)}$$

Where H is hardness, H_0 and K is a constant related to value of hardness and D is crystalline size [20]. The prolonged mixing time leads to excessive plastic deformation of alloyed powders and exposure to the work hardening mechanism, which leads to raises the hardness and brittleness of powders and causes them to show higher hardness values [21]; furthermore, the B_4C particles with longer mixing time dispersed homogeneously through the matrix, which means more diffusion of hardening powders, and also increased the density of dislocation, as a results increment of hardness values of final alloys [12]. Lokesh and Karunakara [22] obtained the same results, where they found that the hardness of Al-Cu/B_4C alloys increased with a prolonged milling time.

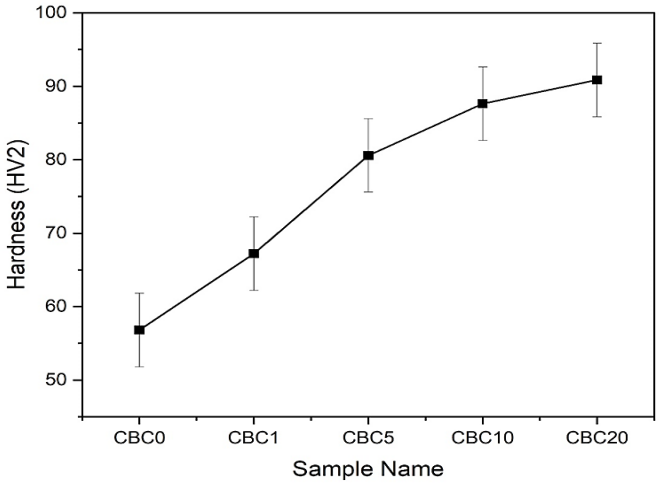

Figure 6. Effect of milling time on hardness

Figure 7 presents the effect of mixing time on the electrical conductivity of Cu-B_4C alloy. As can be seen from the charts, the electrical conductivity decreased from 63% IACS to 25% IACS. The electrical conductivity of Cu-B_4C alloy lowered by about 2.5 times compared to sample without mixing. This can be related to the increasing in porosity which means more void that filled with air inside microstructure which act as isolators of electrical conductivity, also the lattice strain and presence of more-fine ceramic (B_4C) particles due to prolonger mixing time [23]. And as the B_4C has extremely low conductivity, the Cu matrix conductivity continuity broken as B_4C particles networks are formed as a result of more homogenous diffusion through the Cu matrix which is occur with prolonging mixing time [24]. These results align with the literature of Guo et al [25], where they succeeded in decreasing the electrical conductivity of Cu-CrB_2 alloys with longer mixing times. Altinsoy et al [26] observed a decrease in the electrical conductivity of copper when B_4C was added, they attributed this result to the increase in porosity within the copper matrix, which led to a decrease in both relative density and overall density. Thus, this higher porosity acted as an insulation barrier, hindering the passage of electrons between the grains of the copper matrix.

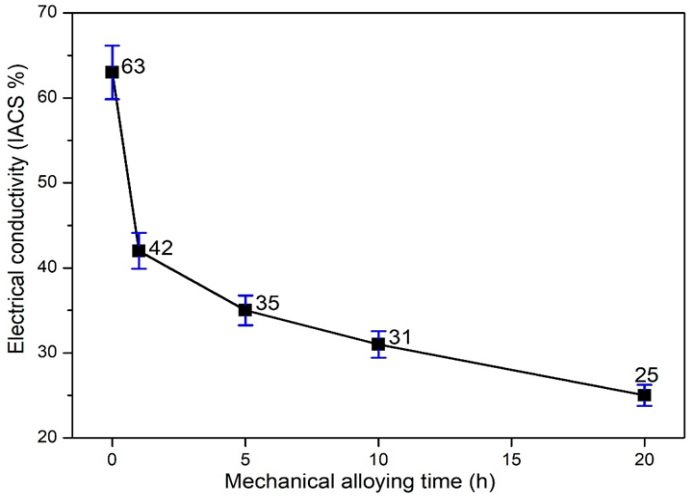

Figure 7. Effect of mechanical alloying time on electrical conductivity

4. Conclusion

The following outcomes were obtained when investigating the effect of milling time on the properties of a Cu matrix composite reinforced with B_4C, fabricated by powder metallurgy approach.

Microstructure inspection showed that as milling time progressed, the microstructure became more homogeneous and the grain became finer due to the work welding effect. At 20 hours of mixing, a steady-state was achieved, where the work welding and fraction effect were almost at the same level. This resulted in a more uniform microstructure and better diffusion of reinforcement particles throughout the matrix. These results were also supported by EDS analysis and mapping images in addition to the calculation of crystallite size.

With an extended milling time, a reduction in both experimental and relative densities occurred, along with an increase in porosity. However, there was a considerable improvement in hardness values. The electrical conductivity gradually decreased with increasing milling time.

Conflict of Interest

All authors certify that they have no affiliations with or involvement in any organization or entity with any financial interest or non-financial interest in the subject matter or materials discussed in this manuscript.

Ethics Committee Approval

Ethics committee approval is not required.

Author Contribution

Conceptization: HH, SI, AOC; methodology and laboratory analyzes: HH; writing draft: HH, SI, AOC; proof reading and editing: HH, SI, AOC. Other: All authors have read and agreed to the published version of the manuscript.

Acknowledgements

This study was funded by project number 1919B012218302 within the scope of the 2209-A University Students Research Projects Support Program, carried out by TÜBİTAK Scientist Support Programs Directorate. As the authors, we would like to thank TÜBİTAK for their support.

5. References

[1] Taya, M., & Arsenault, R. J. (1989). Introduction. In Elsevier eBooks (pp. 1–8).

[2] Şimşek, İ. (2019). The effect of B4C amount on wear behaviors of Al-Graphite/B4C hybrid composites produced by mechanical alloying. Journal of Boron, 4(2), 100-106.

[3] Pripanapong, P., & Tachai, L. (2010). Microstructure and mechanical properties of sintered Ti-Cu alloys. Advanced Materials Research, 93, 99-104.

[4] Chandrakanth, R. G., Rajkumar, K., & Aravindan, S. (2009). Fabrication of copper–TiC–graphite hybrid metal matrix composites through microwave processing. The International Journal of Advanced Manufacturing Technology, 48(5–8), 645–653.

[5] Hamid, F. S., A. Elkady, O., Essa, A. R. S., El-Nikhaily, A., Elsayed, A., & Eessaa, A. K. (2021). Analysis of microstructure and mechanical properties of bi-modal nanoparticle-reinforced Cu-matrix. Crystals, 11(9), 1081.

[6] Fathy, A., & El-Kady, O. (2013). Thermal expansion and thermal conductivity characteristics of Cu–Al2O3 nanocomposites. Materials & Design (1980-2015), 46, 355-359.

[7] Shaik, M. A., & Golla, B. R. (2020). Mechanical, tribological and electrical properties of ZrB2 reinforced Cu processed via milling and high-pressure hot pressing. Ceramics International, 46(12), 20226-20235.

[8] M.Rohini, P.Reyes, S.Velumani, and Becerril J. I. G. (2014). Effect of Milling Time on Mechanically Alloyed Cu(In,Ga)Se2 Nanoparticles, in 2014 11th International Conference on Electrical Engineering, Computing Science and Automatic Control (CCE), , pp. 413–417.

[9] Akbarpour M. R. (2021). Effects of mechanical milling time on densification, microstructural characteristics and hardness of Cu–SiC nanocomposites prepared by conventional sintering process. Mater Chem Phys, vol. 261, Mar.

[10] StandardTest Methods for Density of Compacted or Sintered Powder Metallurgy (PM) Products Using Archimedes' Principle1. 2008.

[11] Gogebakan, M., Kursun, C., & Eckert, J. (2013). Formation of new Cu-based nanocrystalline powders by mechanical alloying technique. Powder technology, 247, 172-177.

[12] Salur, E., Acarer, M., & Şavkliyildiz, İ. (2021). Improving mechanical properties of nano-sized TiC particle reinforced AA7075 Al alloy composites produced by ball milling and hot pressing. Materials Today Communications, 27, 102202.

[13] Liu, G. F., & Chen, T. J. (2022). Effect of ball-milling time on microstructures and mechanical properties of heterogeneity-improved heterostructured 2024Al alloys fabricated through powder thixoforming. Materials Chemistry and Physics, 291, 126684.

[14] Toozandehjani, M., Matori, K. A., Ostovan, F., Abdul Aziz, S., & Mamat, M. S. (2017). Effect of milling time on the microstructure, physical and mechanical properties of Al-Al2O3 nanocomposite synthesized by ball milling and powder metallurgy. Materials, 10(11), 1232.

[15] Zhou, J., & Duszczyk, J. (1999). Liquid phase sintering of an AA2014-based composite prepared from an elemental powder mixture. Journal of materials science, 34(3), 545-550.

[16] Kriewah, O. A. E., & Islak, S. (2022). Synthesis of Cu-Cr-B4C-CNF hybrid composites. Kastamonu University Journal of Engineering and Sciences, 8(2), 90-97.

[17] Asghar, Z., Latif, M. A., Rafi-ud-Din, Nazar, Z., Ali, F., Basit, A., ... & Subhani, T. (2018). Effect of distribution of B4C on the mechanical behaviour of Al-6061/B4C composite. Powder Metallurgy, 61(4), 293-300.

[18] Rahimian, M., Ehsani, N., Parvin, N., & reza Baharvandi, H. (2009). The effect of particle size, sintering temperature and sintering time on the properties of Al–Al2O3 composites, made by powder metallurgy. Journal of Materials Processing Technology, 209(14), 5387-5393.

[19] Şevik, H., & Kurnaz, S. C. (2006). Properties of alumina particulate reinforced aluminum alloy produced by pressure die casting. Materials in Engineering, 27(8), 676–683.

[20] Alizadeh, A., & Taheri-Nassaj, E. (2012). Mechanical properties and wear behavior of Al–2wt.% Cu alloy composites reinforced by B4C nanoparticles and fabricated by mechanical milling and hot extrusion. Materials Characterization, 67, 119–128.

[21] Suryanarayana, C. (2001). Mechanical alloying and milling. Progress in materials science, 46(1-2), 1-184.

[22] Lokesh, G. N., & Karunakara, S. (2020). Impact of Particle size distribution for variable mixing time on mechanical properties and microstructural evaluation of Al-Cu/B4C composite. Materials Today: Proceedings, 22, 1715-1722.

[23] Shukla, A. K., Nayan, N., Murty, S. V. S. N., Sharma, S. C., Chandran, P., Bakshi, S. R., & George, K. M. (2013). Processing of copper–carbon nanotube composites by vacuum hot pressing technique. Materials Science and Engineering: A, 560, 365-371.

[24] Shu, D., Li, X., & Yang, Q. (2021). Effect on Microstructure and Performance of B4C Content in B4C/Cu Composite. Metals, 11(8), 1250.

[25] Guo, X. F., Jia, L., Lu, Z. L., Xie, H., & Kondoh, K. (2024). Enhanced combination of strength and electrical conductivity properties with CrB2 reinforced Cu matrix composites fabricated by powder metallurgy. Materials Today Communications, 38, 107980.

[26] Altinsoy, I., Efe, F. G. C., Aytaş, D., Kılıç, M., Ozbek, I., & Bindal, C. (2013). Some properties of Cu-B4C composites manufactured by powder metallurgy. Periodicals of Engineering and Natural Sciences, 1(1).

doi:10.55385/kastamonujes.1456041 KUJES 10(1):15-21, 2024

Kastamonu University
Journal of Engineering and Sciences
e-ISSN 2667-8209
http://dergipark.gov.tr/kastamonujes

Towards Sustainable Urban Transformation: The Role of LEED Certification in Istanbul's Future and Economy

Oğuzhan Toğay

Department of Civil Engineering, Faculty of Engineering and Architecture, Izmir Katip Celebi University, Izmir, Türkiye

Corresponding Author: oguzhan.togay@ikcu.edu.tr

Received: **March 20, 2024** ◆ Accepted: **May 13, 2024** ◆ Published Online: **June 28, 2024**

Abstract: Istanbul, a city with a rich history and vibrant culture, faces the imminent threat of a catastrophic earthquake due to its proximity to the North Anatolian Earthquake Fault. In response, the Turkish government has initiated a sweeping urban transformation led by the Ministry of Environment and Urbanization. This initiative aims to not only rebuild the city but also to enhance its resilience to earthquakes and environmental challenges. Central to this transformation is the adoption of green building principles, particularly LEED (Leadership in Energy and Environmental Design) certification. LEED provides a comprehensive framework for sustainable building design, construction, and operation, encompassing categories such as Sustainable Sites, Water Efficiency, Energy and Atmosphere, Materials and Resources, Indoor Environmental Quality, Innovation, and Regional Priority. This paper examines the economic and future considerations of enforcing green certification during Istanbul's urban transformation. Through a detailed analysis of the costs and benefits of LEED certification across different categories, as well as alternative approaches to sustainability, this paper aims to provide a holistic view of the implications for Istanbul's economic landscape and long-term prospects. By integrating environmental sustainability into its urban renewal efforts, Istanbul has the opportunity to not only mitigate the risks of earthquakes but also to emerge as a model for sustainable, environmentally conscious urban development. This paper seeks to highlight the importance of green certification in shaping Istanbul's urban landscape for generations to come, with a focus on economic considerations, environmental impacts, and broader implications for the city's future.

Keywords: Urban transformation, LEED certification, sustainability, economic considerations

Öz: İstanbul, zengin bir tarihe ve canlı bir kültüre sahip bir şehir olup, Kuzey Anadolu Fay Hattı'na yakınlığı nedeniyle yakın bir gelecekte büyük bir deprem tehdidi ile karşı karşıyadır. Türk hükümeti, bu tehdide yanıt olarak Çevre ve Şehircilik Bakanlığı öncülüğünde kapsamlı bir kentsel dönüşüm başlatmıştır. Bu girişim, sadece şehri yeniden inşa etmeyi değil, aynı zamanda depremlere ve çevresel zorluklara karşı direncini artırmayı amaçlamaktadır. Bu dönüşümün merkezinde, özellikle LEED (Energy and Environmental Design'da Liderlik) sertifikasyonu olmak üzere yeşil bina prensiplerinin benimsenmesi yer almaktadır. LEED, sürdürülebilir bina tasarımı, inşaatı ve işletmesi için kapsamlı bir çerçeve sunmakta olup, Sürdürülebilir Siteler, Su Verimliliği, Enerji ve Atmosfer, Malzeme ve Kaynaklar, İç Ortam Kalitesi, İnovasyon ve Bölgesel Öncelik gibi kategorileri içermektedir. Bu makale, İstanbul'un kentsel dönüşümü sırasında yeşil sertifikasyonun ekonomik ve geleceğe dönük boyutlarını ele almaktadır. LEED sertifikasyonunun farklı kategorilerdeki maliyetlerinin ve faydalarının detaylı bir analizi ile birlikte, sürdürülebilirliğe alternatif yaklaşımlar da incelenerek, bu makale İstanbul'un ekonomik manzarası ve uzun vadeli perspektifleri için bütüncül bir bakış sunmayı amaçlamaktadır. Çevresel sürdürülebilirliği kentsel yenileme çabalarına entegre ederek, İstanbul, deprem risklerini azaltmanın yanı sıra sürdürülebilir, çevre dostu kentsel gelişim için bir model olarak da ortaya çıkma fırsatına sahiptir. Bu makale, İstanbul'un kentsel peyzajını gelecek nesiller için şekillendirmede yeşil sertifikasyonun önemini vurgulamayı amaçlamaktadır, bunu yaparken ekonomik değerlendirmeler, çevresel etkiler ve şehrin geleceği için daha geniş çıkarımlara odaklanmaktadır.

Anahtar Kelimeler: Kentsel dönüşüm, LEED sertifikasyonu, sürdürülebilirlik, ekonomik değerlendirmeler

1. Introduction

Istanbul, a city full of life and history, rests uneasily near a North Anatolian Earthquake Fault (Figure 1). A powerful earthquake bigger than 7.2 could potentially hit the city. Responding to this risk, the Turkish government has initiated an ambitious urban transformation led by the Ministry of Environment and Urbanization.

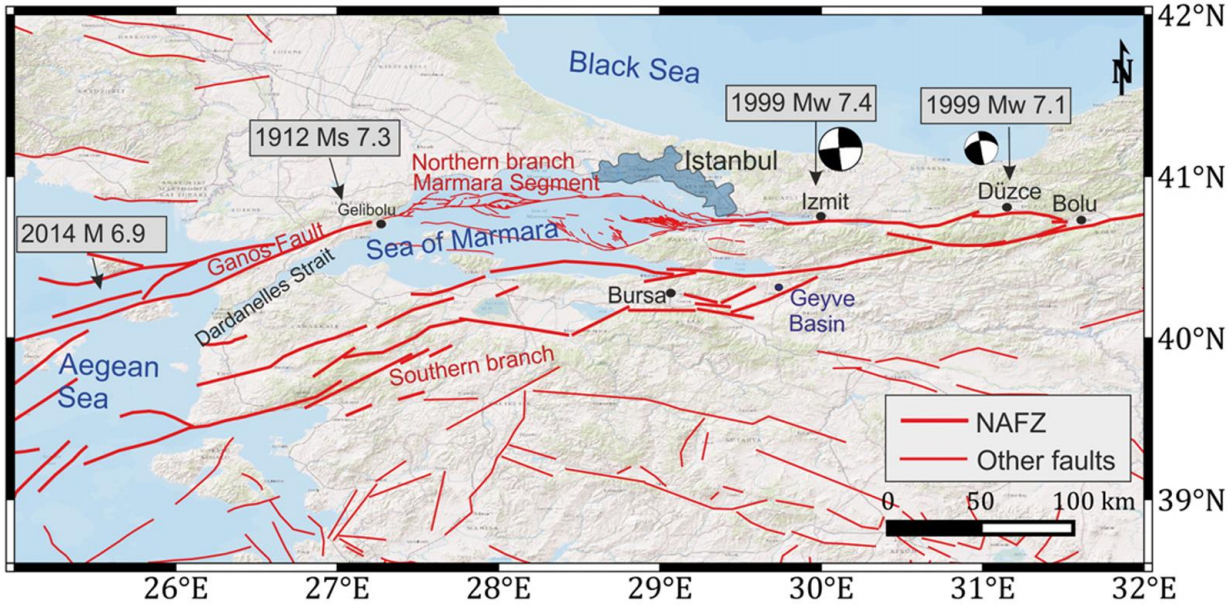

Figure 1. North Anatolian Fault Zone Istanbul and Marmara Sea Area, adapted from Bohnhoff et al [1]

This initiative goes beyond mere physical reconstruction, aspiring to safeguard lives and enhance earthquake resilience. The scale is significant: over 232,000 buildings across Istanbul urgently need reconstruction and risk collapsing during the expected earthquake [2].

However, the imperative for change extends beyond physical reconstruction. Erecting new structures on shaky foundations falls short of genuinely fortifying Istanbul. A comprehensive approach is necessary, involving comprehensive city planning, robust infrastructure development, and careful disaster preparedness. This vision is not just about reinforcing buildings; it's about empowering communities to endure earthquakes and emerge more resilient.

The ongoing urban transformation also provides an opportunity to integrate environmental sustainability into Istanbul's renewal. By incorporating green building principles such as energy efficiency, water conservation, renewable energy use, and pollution reduction, Istanbul can become a city resilient to earthquakes and environmentally conscious.

In this context, the discussion in this paper revolves around the concept of forcing green certification during urban transportation. The paper delves into the positives and negatives of this approach concerning Istanbul's economy and future. The notion of imposing green certification, explored against the backdrop of the city's seismic concerns and ongoing urban transformation, is crucial for understanding the potential impacts on Istanbul's economic landscape and long-term prospects.

The concept of green buildings, which began in Turkey in the early 2000s, has already made progress. Growing awareness in both the public and private sectors, particularly in recent years, is driving this advancement. Embracing green building practices is key to achieving Turkey's sustainable development goals, and Istanbul's transformation is fertile ground for their implementation.

In essence, Istanbul's urban transformation is more than just rebuilding structures. It can be a catalyst for creating a future that is earthquake-resistant, climate-resilient, and environmentally responsible. By combining community empowerment, green building principles, and sustainable development, Istanbul has the opportunity to stand tall not only during earthquakes but also as a sustainable and environmentally friendly city, with the discussion on forcing green certification adding an additional layer to the city's economic and future considerations.

2. Methodology and Research Design

In this paper, the economic and future considerations for the urban transformation considering the green building certification are examined. For this purpose, the building stock of the city of Istanbul is examined and checked for each category on the LEED® certification. For categories, not all the subsections are examined but the main category is observed in order to understand the economic effects of it particularly.

LEED® Categories for new construction and renovation on Istanbul Urban Transformation

Sustainable Sites

According to the U.S Green Building Council LEED® documentation, this section is giving one point each if the below considerations are addressed:

•Site Development – Protect or Restore Habitat

In alignment with the vision of the Turkish Ministry of Environment and Urbanization, prioritizing reconstruction on existing building sites minimizes habitat disturbance and promotes resource efficiency. This approach aligns with the Ministry's goals and reduces environmental impact without incurring additional economic burdens. However, a thorough environmental impact assessment remains crucial to identify and mitigate any potential negative impacts on sensitive habitats, even within existing footprint areas.

•Site Development – Maximize Open Space

The urban transformation plan encourages the consolidation of smaller building plots into larger sites. This strategy presents a cost-neutral approach to maximizing open space within the transformed urban landscape. By consolidating plots, opportunities arise for the creation of more extensive, interconnected green areas, parks, plazas, or other community spaces, potentially enhancing quality of life and environmental benefits without incurring additional development costs. However, careful consideration should be given to potential challenges, such as ensuring equitable access to open space for all residents, balancing individual property rights with community needs, and mitigating potential social disruptions associated with land consolidation.

•Stormwater Design – Quantity Control and Stormwater Management – Quality Control

This study considers both stormwater quantity and quality control measures within the existing urban infrastructure. This approach leverages the current system, potentially allowing for points to be earned without incurring additional capital expenditure. However, further investigation is required to assess the adequacy of the existing infrastructure to meet all regulatory requirements and desired performance standards.

•Heat Island Effect – Nonroof and Roof

Recent research highlights by to Baykara [3], Istanbul's intensifying heat island effect, posing significant challenges for urban inhabitants. However, emerging evidence suggests that this issue can be addressed through urban transformation projects without incurring additional costs. By strategically integrating heat mitigation strategies into these initiatives, a significant cooling effect can be achieved.

Water Efficiency

•Water Efficient Landscaping

Integrating water-efficient landscaping strategies into urban transformation initiatives presents unique challenges. Retrofitting existing infrastructure often proves more complex and costly compared to incorporating sustainability features in new builds. While initial investments in technology and installation might be higher, the potential for long-term water savings, especially considering the often-large scale of urban transformation projects, necessitates a closer examination of the cost-benefit analysis.

•Innovative Wastewater Technologies

Effective water management strategies are crucial for successful urban transformation, demanding attention at both individual buildings and city-wide levels. At the individual level, implementing rainwater harvesting systems for irrigation and separating greywater (excluding kitchen wastewater) from blackwater offers numerous benefits. These include reduced reliance on potable water, minimized strain on centralized treatment facilities, and potential resource recovery like nutrient recycling from greywater.

On a city-wide scale, large-scale implementation of filtration systems for treated sewage and rainwater holds significant promise. This contributes to improved water quality discharged into receiving bodies, mitigating potential environmental and public health impacts associated with untreated wastewater. While upfront costs are associated with installing these systems, their long-term economic benefits through reduced water consumption and avoided environmental damage warrant thorough evaluation. Additionally, social factors like public acceptance and equitable access to resources must be carefully addressed. Overall, prioritizing sustainable wastewater management through rainwater harvesting, greywater separation, and large-scale filtration presents a powerful opportunity to enhance the environmental and social outcomes of urban transformation projects.

Energy and Atmosphere

The Leadership in Energy and Environmental Design (LEED) certification system emphasizes sustainable building practices, with the Energy and Atmosphere (EA) category playing a crucial role in promoting energy efficiency and reducing environmental impact. This section accounts for up to 40 points within the overall LEED score, signifying its substantial influence on achieving certification. The EA category focuses on reducing a building's energy consumption and its associated environmental consequences. By implementing strategies outlined within the EA credits, buildings can achieve significant improvements in energy performance, leading to reduced operational costs, decreased greenhouse gas emissions, and enhanced occupant comfort and health.

The specific requirements of the EA category delve into various aspects of building design and operation that influence energy consumption. These include building envelope performance, high-performance windows and doors, energy-efficient HVAC systems, and lighting systems. While the EA category encompasses various aspects of building energy use, it excludes the specific minimum efficiencies required for home appliances, as these are typically left to the discretion of individual owners. By prioritizing energy performance throughout the design, construction, and operation phases, buildings can contribute to a more sustainable and resilient future for cities like Istanbul undergoing significant urban transformation. The considerations highlighted within the EA category offer a valuable framework for guiding the development of energy-efficient buildings within this context.

Considering Istanbul's ongoing urban transformation, the cost associated with implementing the EA measures in this section is estimated to range from $1,000 to $1,500 per unit, according to Schifman [4]. With an estimated 292,000 buildings requiring this transformation, each containing an average of 10 individual units, the total number of units requiring intervention reaches 2,922,000. Assuming the most cost-effective option of $1,000 per unit, the total estimated cost for implementing these measures across Istanbul's buildings would be approximately $2,922,000,000.

However, it is crucial to acknowledge that this initial investment is expected to be offset over time through reduced energy consumption and associated cost savings. Additionally, the positive impact on public health due to improved indoor air quality and occupant comfort should be factored into the overall economic evaluation.

Materials and Resources

The Materials and Resources section of LEED certification focuses on three key sustainability aspects:

-Environmentally Friendly Materials: This credit encourages the use of materials with reduced environmental impact throughout the construction process.

-Reducing Construction and Demolition Waste: This credit emphasizes strategies to minimize waste generation during construction and demolition activities.

-Building Durability and Resilience: This credit promotes the design and construction of buildings with enhanced durability and resilience to withstand natural disasters and extreme weather events.

Given Istanbul's location within the seismically active North Anatolian Fault zone (Figure 1), durability becomes a paramount concern during urban transformation. Implementing measures to enhance building resilience against earthquakes is crucial to prevent catastrophic consequences similar to those witnessed in the 1999 Düzce earthquake and the 2023 Hatay and Kahramanmaraş earthquakes. However, achieving this objective without incurring significant additional costs requires careful consideration.

The selection of construction materials inevitably impacts the environment. While minimizing environmental impact is desirable, it is essential to acknowledge the current limitations and infrastructure realities within Istanbul. The widespread use of reinforced concrete in recent Turkish construction projects presents challenges in transitioning to alternative materials like steel or timber structures. This shift might be hindered by the potential lack of a readily available skilled workforce accustomed to working with these alternative materials. Consequently, a detailed cost analysis considering both environmental and economic factors is necessary before implementing significant changes in material selection.

While opportunities for minimizing waste from existing buildings might be limited, strategies can be employed to reduce waste generation during the demolition and reconstruction phases. Reusing existing reinforcement materials from demolished structures after appropriate processing offers a viable solution that can contribute to both cost savings and environmental benefits.

The Materials and Resources section presents significant opportunities to promote sustainability within Istanbul's urban transformation. However, a balanced approach that prioritizes earthquake resilience, economic feasibility, and environmental considerations is crucial for successful implementation.

Indoor Environmental Quality

Over the past two decades, Istanbul has experienced a notable enhancement in its air quality, largely credited to the increased adoption of natural gas for residential heating purposes. The improvement is evident in Table 1, which outlines the air quality index and other relevant parameters for 2023 for the districts of the city of Istanbul. Throughout the year, the air quality index consistently registers below 50 across most districts, indicating that the air quality concern in residential areas primarily stems from internal sources, which consequently impacts the overall air quality negatively. To combat this issue, integrating in-house air filters and purifiers with existing air conditioning systems emerges as the most viable solution. However, during winter, the city's air quality index sees a significant rise, necessitating the use of air purifiers and filtration systems for entire buildings. The cost of an air purifier per unit is approximately $300, and with an estimated 2,992,000 units required, the total cost for implementing this solution would amount to around 900 million dollars.

Table 1. Istanbul air quality data from 2023 (1.1.2023 – 31.12.2023), Data is obtained from the Istanbul Metropolitan Municipality Air Quality Department [5]

Station	Air Pollution Index	PM10 (µg/m³)	PM25 (µg/m³)	SO_2 (µg/m³)	CO (µg/m³)	NO (µg/m³)	NO2 (µg/m³)	NOX (µg/m³)	O_3 (µg/m³)
Şile	32	22.5	-	9.2	-	2.9	8.3	13.1	71
Kumköy	24	20.7	5.7	-	322	15.4	21.5	54.8	24.3
Büyükada	17	17.8	-	-	-	-	-	-	12.9
Kandilli 2	27	29.5	-	19.1	1516.2	36.9	33	91.7	-
Silivri	39	29.8	16	7.5	-	6.9	17	28.2	76.5
Esenler	32	33.1	20.3	3.4	558.5	41.3	42.8	106.9	33.3
Kağıthane 2	22	-	19.4	12.3	-	38	43.3	102.1	36.4
Esenyurt	44	54	-	20.5	-	36.2	40.1	96.1	45.8
Yenibosna	27	48.3	-	2.1	693.7	40.3	42.5	104	-
Sultanbeyli	32	30.5	-	22	-	22.7	34.2	69	60.2
Kadıköy	33	33.3	21.1	3.6	604.3	42.7	38.7	103.9	36.1
Alibeyköy	38	32	18.8	4.8	521.7	103.9	43.8	212.2	18.1
Kartal	39	53	28.9	3.7	556.2	38.9	42.2	102.1	34.7
Bağcılar	33	38.6	21.7	2.9	543	25.4	42.5	81.4	36.1
Sarıyer	37	21.8	-	3.9	-	24.1	29.6	66.4	42.4
Sancaktepe	39	47.7	-	4.5	597.1	22.1	30.9	64.3	42.1
Tuzla	39	47.8	20	5.4	366.7	39.6	44.4	105.4	20.5
Üsküdar 1	37	26.3	12.5	2.5	-	15.1	33.7	55.4	-
Kağıthane 1	42	57.9	21.3	5.8	536.8	41.4	34	102.9	12.6
Arnavutköy	32	32.6	18	3.5	393.3	9.7	21.6	36.4	44.5
Başakşehir	36	41.8	-	25.7	1671.1	15.1	29.6	52.6	53.3
Ümraniye 2	42	35.6	16	13.8	6014.8	52.5	49.3	130.5	-
Üsküdar 2	32	35.8	-	-	-	34.2	41.3	94.5	-
Aksaray	45	40.5	21.8	3.7	728.9	104.3	77.6	237.2	13.3
Şirinevler	38	36.8	-	3.8	1231.9	32.8	65.1	116.1	-
Beşiktaş	38	38.1	20	3.8	513.3	42.4	50.8	115.4	26
Mecidiyeköy	30	53.5	-	-	1928.5	80.5	26.2	150.3	-
Selimiye	37	45.8	26.6	-	479.3	30.5	22.7	68.6	40.4
Göztepe	59	90	-	-	1061.4	67.6	68.2	171.6	-
Çatladıkapı	28	31.3	17.9	-	603.6	27.3	40.3	82.7	36
Maslak	28	30.6	15.4	3	-	26.3	20.9	62.1	27.4
Ümraniye 1	52	44.9	28.5	3.8	-	14.3	31.8	56.8	36
Avcılar	26	26.4	17.6	3.1	-	8.3	27.6	41.9	33
Kandilli 1	13	14.9	-	-	-	-	-	-	14.8
Average	35	38.4	19.4	7.6	1021.1	35.6	37.4	93	36.5

Innovation and Regional Priority

Although this category of LEED certification requires mostly individual solutions for the buildings, forcing the contractors to follow LEED innovation catalog [6] can easily help the buildings receive the points that can be obtained from the Innovation section. Since this section is more subjective with respect to the contractor, the cost of the application for this part is not included in the overall system.

For regional priority, according to v4.1 of the LEED rating system, each individual location can be accessed and checked for extra points. Since this part is specific to buildings this part is also left out for the cost calculations.

Application and Other Costs

The LEED rating system entails more than just registration; it also involves payment for third-party testing and final verification. The total cost breakdown is detailed below in Table 2.

Table 2. Registration fees break downs for residential areas. Data is obtained for certification for out of United States Section [7]

Building Design and Construction fees per building	**Silver, Gold and Platinum level members**	
Registration	$1,350	
Precertification		
Flat fee (per building)	$4,500	
Combined Certification Review: Design and Construction	Rate	Minimum
Project gross floor area (excluding parking): less than 24,000m^2	$0.695/m^2	$3,200
Project gross floor area (excluding parking): 24,000m^2 - 48,000 m^2	$0.674/m^2	$16,000
Project gross floor area excluding parking): 48,000m^2 - 72,000m^2 sq ft	$0.608/m^2	$31,000

Since the problematic buildings are mostly fit in the first bullet, which is "Project gross floor area (excluding parking): less than 24,000m^2" and the areas are less than 5,000 m^2, the average certification review cost is taken as $3,500. Adding Registration and Flat fee on top of the certification review cost makes the total of $9,350. Considering 292,000 buildings, the total cost for the project using LEED certification for all the urban transformation areas makes $2,730,200,000.

3. Conclusion

In conclusion, Istanbul's urban transformation represents a critical opportunity to not only rebuild the city but also to create a more resilient, sustainable, and environmentally conscious urban environment. The city's seismic risks, highlighted by its proximity to the North Anatolian Earthquake Fault, underscore the importance of holistic and forward-thinking approaches to urban development.

The LEED certification process, while presenting significant upfront costs, offers a framework for achieving these goals. By incorporating green building principles across categories such as Sustainable Sites, Water Efficiency, Energy and Atmosphere, Materials and Resources, Indoor Environmental Quality, Innovation, and Regional Priority, Istanbul can not only enhance its earthquake resilience but also improve its overall quality of life for residents.

While the total cost of LEED certification may seem prohibitive, the long-term benefits, including improved life quality, reduced health hazards, and a more sustainable future, far outweigh the initial investment. Moreover, the potential savings in energy costs and environmental impact mitigation contribute to the economic viability of the certification process.

4. Total Breakdown

When considering the total cost breakdown of LEED certification for Istanbul's urban transformation, including Certification and Review, Indoor Environmental Quality, Energy and Atmosphere, and other associated costs, the total amount reaches $5,653,100,000. While this cost is substantial, the benefits in terms of improved life quality, reduced health hazards, and a sustainable future justify the investment.

An alternative approach could involve not enforcing LEED certification but still implementing green building practices. This could reduce the total cost by approximately $2,730,200,000. However, without certification, the process would need to be overseen by authorities to ensure adherence to sustainability standards.

In conclusion, while the cost of LEED certification for Istanbul's urban transformation is significant, the potential benefits in terms of resilience, sustainability, and quality of life make it a worthwhile investment for the city's future.

Conflict of Interest

All authors certify that they have no affiliations with or involvement in any organization or entity with any financial interest or non-financial interest in the subject matter or materials discussed in this manuscript.

Ethics Committee Approval

Ethics committee approval is not required.

Author Contribution

Conceptization, methodology, laboratory analyzes, writing draft, proof reading and editing: OT.

Acknowledgements

The author would like to acknowledge the support and resources provided by İzmir Katip Çelebi University. The work was carried out independently, and no specific funding was received for this research.

5. References

[1] Bohnhoff, M., Martínez-Garzón, P., Bulut, F., Stierle, E., & Ben-Zion, Y. (2016). Maximum earthquake magnitudes along different sections of the North Anatolian fault zone. Tectonophysics, 674, 147-165.
[2] Municipality İ. M. (2019). İstanbul Deprem Çalıştayı, Istanbul Metropolitan Municipality, İstanbul.
[3] Baykara, M. (2023). An Assessment of Long-Term Urban Heat Island Impact on Istanbul's Climate. International Journal of Environment and Geoinformatics, 10(2), 40-47.
[4] Schifman, M. R. (2020). LEED v4.1 for Homes 101: Translating The Energy & Atmosphere Prerequisites, Rise, 17 December. [Online]. Available: https://www.buildwithrise.com/stories/leed-for-homes-101-energy-and-atmosphere-prerequisites. [Accessed 24 February 2024].
[5] Department, I. M. M. A. Q. (2023). Periodical Air Quality Report, Istanbul Metropolitan Municipality , 31 12 2023. [Online]. Available: 10. [Accessed 3 2024].
[6] Council, U. G. B. (2024). LEED Credit Library, U.S Green Building Council , March 2024. [Online]. Available: https://www.usgbc.org/innovationcatalog. [Accessed 2024].
[7] Council, U. S. G. B. (2024). LEED certification fees, United States Green Building Council , 2024. [Online]. Available: https://www.usgbc.org/tools/leed-certification/fees. [Accessed 2024].
[8] Bayat, F., & Küçükali, U. F. (2021). Sürdürülebilirlik bağlamında yeşil binaların ulusal ve uluslararası örnekler üzerinden incelenmesi. Anadolu Bil Meslek Yüksekokulu Dergisi, 16(64), 321-347.

Kastamonu University
Journal of Engineering and Sciences
e-ISSN 2667-8209
http://dergipark.gov.tr/kastamonujes

Effect of Bone Ash and Rice Husk Ash on the Unconfined Compressive Strength of Silt Soil

Mehmet Uğur Yılmazoğlu

Department of Civil Engineering, Faculty of Engineering and Architecture, Kastamonu University, Kastamonu, Türkiye
Corresponding Author: myilmazoglu@kastamonu.edu.tr

Received: **April 18, 2024** ◆ Accepted: **June 12, 2024** ◆ Published Online: **June 28, 2024**

Abstract: This study investigated the soil stabilization potential of ash obtained from the calcination of cattle bones and ash produced by burning rice husks on silty soil. After the cattle bones were first crushed and burned, they were calcined at 800°C for 1 hour, allowed to cool, ground, and sieved with a sieve with a 75-micrometer opening to obtain bone ash (BA). To get rice husk ash (RHA), rice husks were burned, ground, and sieved through a 75-micrometer aperture. A silt soil sample taken from a depth of 3-4 meters from the center of Sakarya Province in Yenigün District of Adapazarı district was used to stabilize it. RHA was added as ground and unground, 10% by weight of the samples, BA as 7% by weight of the samples, and BA and RHA as 7% BA + 10% RHA by weight of the samples. Unconfined compressive strength (UCS) tests were performed for this research. The results showed that the UCS value increased with the addition of BA and RHA as the curing time increased for 7% BA, 7%BA+10% RHA, and 10% ground RHA, while 10% unground RHA lost strength. Caused Therefore, 7%BA+10%RHA can be used to increase the UCS value of the soil. Instead of allowing bones to be disposed of in the environment, calcined bone ash should be encouraged to sustain people's livelihood on stabilized soils.

Keywords: Sustainability, bone ash, rice husk ash, soil improvement, unconfined compressive strength

Öz: Bu çalışma, sığır kemiklerinin kalsinasyonundan elde edilen kül ile pirinç kabuğunun yakılmasıyla edielien külün siltli zeminin üzerinde zemin sabilizasyon potasiyelinin araştırılmasına odaklandı. Sığır kemikleri öncelikle parçalanarak yakıldıktan sonra 800°C'de 1 saat süreyle calsine edildi, soğumaya bırakıldı, öğütüldü ve kemik külü (BA) elde etmek için 75 mikrometre açıklığa sahip elek ile elendi. Pirinç kabuğu külü (RHA) elde etmek için pirinç kabukları yakıldı, öğütüldü ve 75 mikrometre açıklığa sahip elek ile elendi. Adapazarı ilçesi Yenigün Mahallesi'ndeki Sakarya İli merkezinden 3-4 metre derinlikten alınan silt zemin numunesi stabilize etmek için kullanıldı. RHA öğütülmüş ve öğütülmemiş olarak, numunelerin ağırlığına göre %10, BA, numunelerin ağırlığına göre %7 ve BA ile RHA numunelerin ağırlığına göre %7 BA+%10 RHA olarak eklenmiştir. Bu araştırma için Serbest basınç dayanımı (UCS) testleri yapıldı. Elde edilen sonuçlar, BA ve RHA'nın eklenmesiyle UCS değerinin, %7 BA, %7BA+%10 RHA ve %10 öğütülmüş RHA kürlenme süresi arttıkça artış gösterirken %10 öğütülmemiş RHA dayanım kaybına neden olmuştur. Bu nedenle, %7BA+%10 RHA zeminin UCS değerini artırmak için kullanılabilir. Kemiklerin çevreye atılmasına izin vermek yerine, stabilize topraklarda insanların geçimini sağlamak için kalsine edilmiş kemik külü üretimine girişilmesi teşvik edilmelidir.

Anahtar Kelimeler: Sürüdürülebilirlik, kemik külü, pirinç kabuğu külü, zemin iyileştirme, serbest basınç dayanımı

1. Introduction

Due to rapid urbanization and industrialization on a global scale, waste products diversify every year, and a considerable amount of waste is produced. It is essential to dispose of these waste materials without causing harmful effects on the environment. With the ever-growing environmental problems, the value of the additional material/additive to be used in ground improvement will increase even more if it is environmentally friendly and waste material. When viewed from this perspective, it is evident that rice husk ash (RHA) and animal bones, produced in large quantities in our country and worldwide, will pose a danger as industrial waste if they are not stored properly. Using these industrial (BA, RHA) wastes in ground improvement offers an acceptable environmentally friendly solution.

Bone is a variable tissue that performs many mechanical and biological functions. The main components of bone are amorphous forms of hydroxyapatite and calcium phosphate. The chemical and physical properties of bone are affected by age, nutrition, hormonal status, and diseases [1]. Bone ash (BA) is a whitish powdery residue left over from bone burning (calcination). Ash consists primarily of P_2O_5 and CaO in the form of calcium phosphate ($Ca_3(PO_4)_2$) or modified hydroxyapatite ($Ca_5(PO_4)_3OH$) [2]. The main chemical composition of natural bone is expressed in terms of calcium oxide and phosphorus pentaoxide; for cows, it is 32.1% and 28.3%, respectively.

Rice husk ash (RHA) is a byproduct of burning rice husks. Approximately 150 million tons of rice husks are produced annually worldwide [3-5]. RHA contains about 90% SiO_2 as a large amount of amorphous silica, and many studies are

showing that it can improve the pore structure of concrete and effectively increase the strength and durability of concrete [4-6]. The study investigated the potential for reducing the amount of waste and improving the physical and chemical properties of the soil by using BA and RHA in soil improvement.

2. Material and Method

Adapazarı ground, whose properties are given in Table 1, will be used in the research. Depending on the soil samples' weight, They will be added as 7% BA, 10% RHA, and 7% BA + 10% RHA. The sample was taken from Adapazarı (Turkey), Yenigün District, at a depth of 3-4 m. The properties of the silty soil sample used in this study according to ASTM D4318 [7] are given in Table 1. The soil sample was classified as low plasticity silt (ML) according to USCS. Figure 1 shows the grain size distribution curve of the sample.

Table 1. Physical properties of the soil used in experimental study

Property	Value	Symbol and Unit
No 200#	89	FC (%)
Liquid limit	35	LL (%)
Plastic limit	25	PL (%)
Plasticity index	11	IP (%)
Specific gravity	2,692	G_s
Clay ratio	17	C (%)
Silt ratio	72	M (%)
Sand ratio	11	S (%)
Soil class: Low Plasticity Silt (ML)		

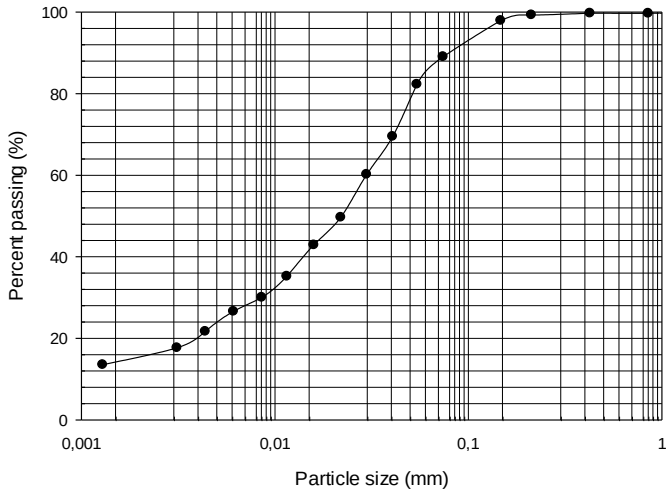

Figure 1. Grain-size distribution of samples used in the study.

First, the optimum water content and maximum dry unit weight of the samples prepared according to the determined mixtures were determined. After the proctor test was prepared at optimum water content, it was cured at 1, 7, and 28-day intervals, and UCS values were determined.

Rice husks are burned industrially in many countries. In addition to providing energy, the combustion process produces rice husk ash, a by-product rich in silica and can be used industrially. While the organic parts are burned away during the burning process, they are protected due to the silica structure specially stored in the shell [8]. For preliminary tests, the chemical properties of the cooled and ground burnt rice husk ash were examined using X-ray fluorescence Spectrometry (XRF) experiments, and the values were obtained in Table 2.

Table 2. Mineralogical properties of the RHA

Symbol	Element	Value(%)
SiO_2	Silicon dioxide	94.05
Al_2O_3	Alumina	0.55
Fe_2O_3	Iron oxide	0.31
MgO	Magnesium oxide	0.88
CaO	Quicklime	0.6
K_2O	Potassium oxide	0.28
Na_2O	Sodium oxide	1.07
SO_3	Sulfur trioxide	0.21
-	Other	2.05

For bone ash (BA), cattle bones taken from the Meat Complex affiliated with Kastamonu Municipality were burned uncontrollably. The chemical properties of BA used in the literature, and the chemical properties of bone ashes were first subjected to burning in the open air for our study, then calcined in the oven at 900 °C for 90 minutes. The ground, after cooling, is shown in Table 3. As can be seen from the table, there is plenty of calcium oxide (CaO) and phosphorus (P_2O_5) in the ash. While CaO increases mechanical strength by providing binding between soil grains, P_2O_5, which is also used as fertilizer in agriculture, will regulate the chemical properties (pH) of the soil.

Table 3. Mineralogical properties of the BA

Symbol	Element	Value (%) England BA	Japan BA	Used in the Study (BA)
CaO	Quicklime	41.7	41.1	54.99
P_2O_5	Phosphorus Pentoxide	57.1	55.9	46.26
SiO_2	Silicon dioxide	0,55	1,38	1.017
Al_2O_3	Alumina	0.33	1.30	< 0,0038
Fe_2O_3	Iron oxide	0.09	0.10	0.1293
Na_2O	Sodium oxide	0.03	0.04	< 0,014
K_2O	Potassium oxide	0.03	0.04	0.032
MgO	Magnesium oxide	0.20	0.21	< 0,0034
TiO_2	Titanium oxide	0.01	0.01	0.00722

In the study, samples will be prepared using BA and RHA materials, which are used to stabilize silty soil. For the stabilization of the soil, BA and RHA, which are not used in the literature, were used as optimum ratios of 7% and 10% of the soil weight, respectively [9–14]. 7% BA + 10% RHA of the soil weight was added.

The experimental study consists of 4 stages. The experimental research defined two materials, three different mixing ratios, and RHA as ground and unground variables. The experimental design using all variables is given in Table 4. First, to find the optimum water content of the mixtures, the optimum water content of the sieved soils was determined by the standard proctor test, considering the maximum grain diameter of the air-dry soil (Figure 2). Mixtures produced at optimum water contents (BA and RHA were thoroughly mixed with soil) were formed using the static compression method to form cylindrical samples with a diameter of 50 mm and a height of 100 mm. After the curing periods, the prepared samples were subjected to the unconfined compressive strength (UCS) test.

Table 4. Mixture properties and experimental design

Mix No.	(%) BA	(%) RHA
1 (Ref.)	0	0.
2	7 (Ground)	0
3	0	10 (Ground)
4	0	10 (Unpılverised)
5	7 (Ground)	10 (Ground)

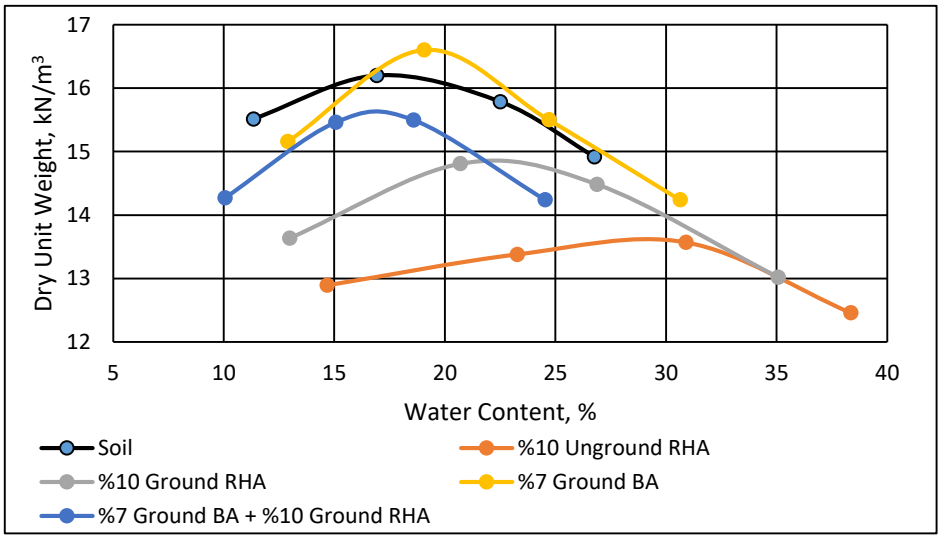

Figure 2. Optimum water content versus the dry unit weight of examples.

The silty soil taken from Adapazarı/Turkey city center was first air-dried in the laboratory environment. The air-dried sample was pulverized by hand. To prepare the samples homogeneously at the desired water content, it was sieved through

the No.10 (2 mm) sieve with the maximum grain diameter to prevent lumping and re-move organic substances. The sieved soil sample was wetted by spraying deionized and deaired water for the desired degree of saturation in groups of 2 kg and mixed with the help of a sample preparation mixer. This process was repeated for each sample of different BA and RHA values. After the prepared samples, three different samples were taken from the other parts to check the WC, and it was confirmed that the water contents of the mixtures in all the prepared samples were equal within ± 0.5% evaporation/moisture change margin of error.

3. Result

The produced BA and RHA were thoroughly mixed with soil and then compacted using the static compaction method to form cylindrical samples with a diameter of 50 mm and a height of 100 mm. Before the UCS test, stabilized soil samples were wrapped with a thin film and cured under standard room conditions (20 ± 2 ˚C) for 1, 7, and 28 days. UCS testing was performed at a 1 mm/min loading rate using the Wykeham Farrance universal testing machine. Three replicates were performed for each mixture in the UCS test [15]. The strength values in Table 5 represent the average of three test results (q_u).

Table 5. Unconfined compressive strength test results of the soil

	Mix No.	Curing time		
		1.Day q_u (kPa)	**7.Day q_u (kPa)**	**28. Day q_u (kPa)**
1	Ref.	57.53	57.53	57.53
2	%7 ground BA	54.96	55.89	70.96
3	%10 unground RHA	54.82	57.85	68.79
4	%10 ground RHA	34.13	37.14	40.44
5	%7 ground BA + %10 ground RHA	61.18	71.44	110.26

The maximum unconfined compressive strength values (qu) of each mixture according to their curing times are shown in Figure 3. Looking at Figure 3, qu strength increased as the curing time increased in all mixtures. In the mix where only unmilled rice husk was used, strength was lost compared to the reference sample value.

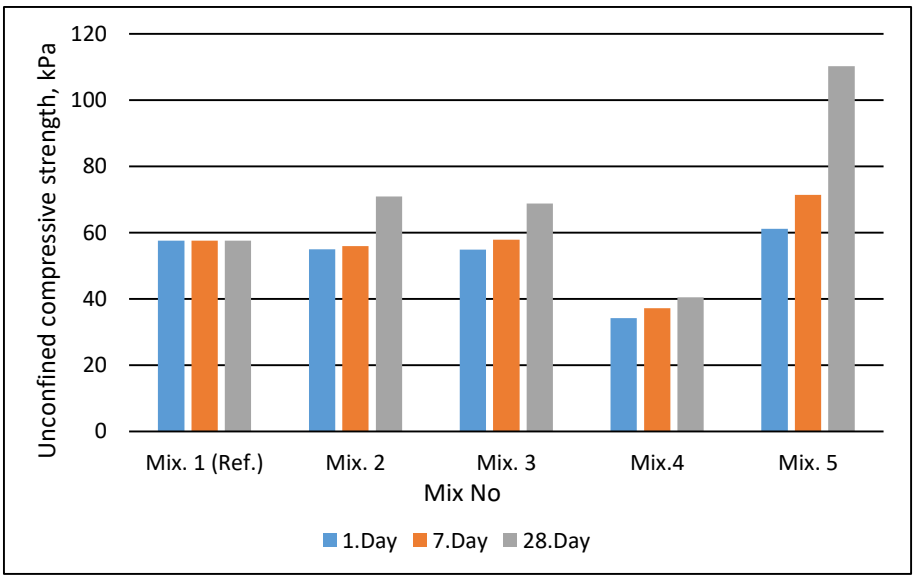

Figure 3. UCS versus curing time comparison

Unconfined compressive strengths were recorded as a function of vertical displacement up to the maximum value (Figure 4-7).

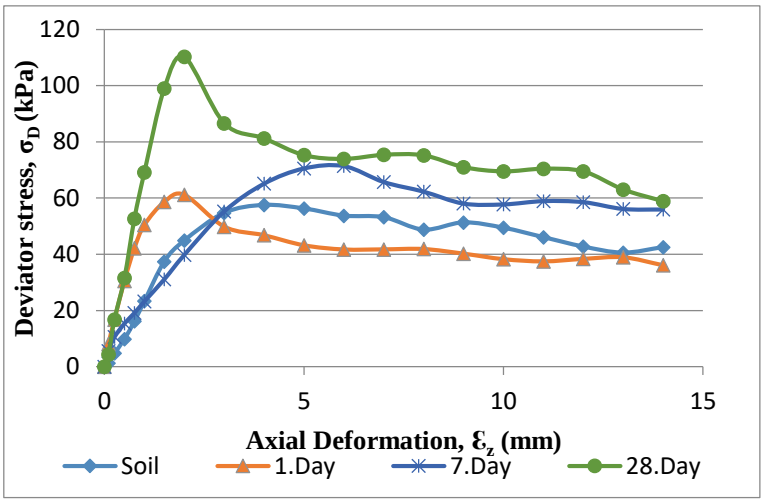

Figure 4. qu versus axial deformation relations under different curing times of %7 ground BA + %10 ground RHA mix

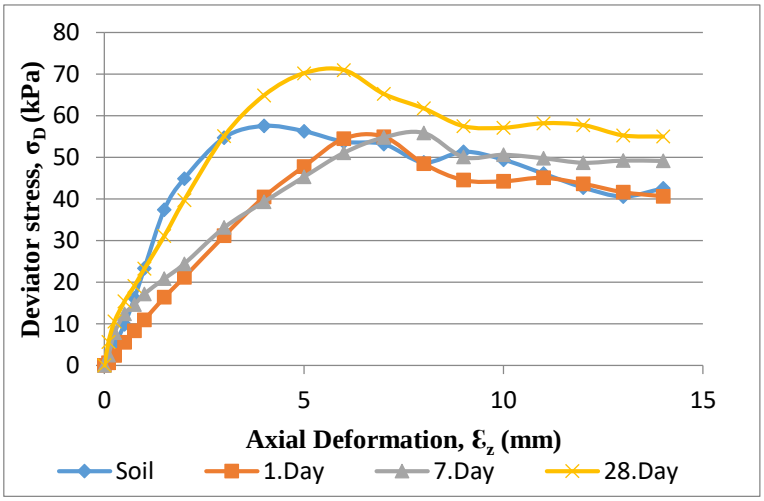

Figure 5. qu versus axial deformation relations under different curing times of %7 ground BA mix

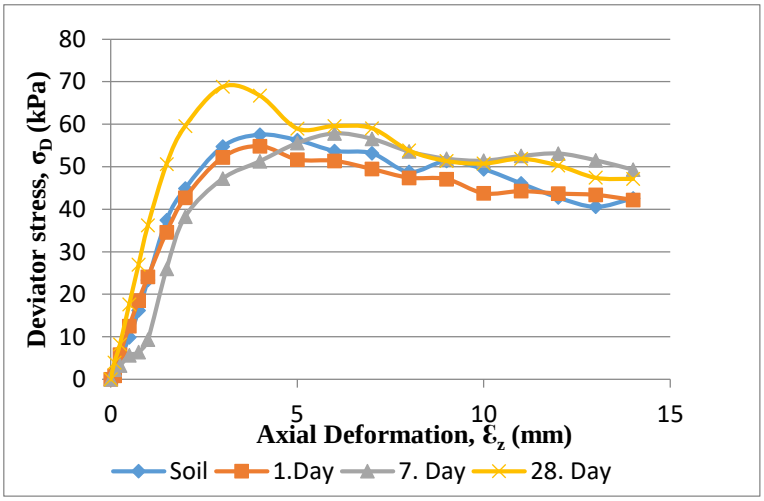

Figure 6. qu versus axial deformation relations under different curing times of %10 ground RHA mix

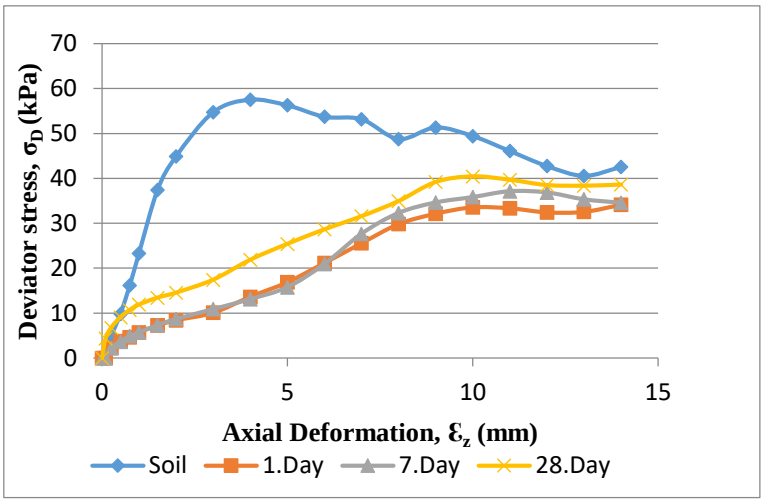

Figure 7. qu versus axial deformation relations under different curing times of %10 unground RHA mix

4. Discussion and Conclusion

There are very few studies in which BA and RHA are used together in studies aimed at improving the unconfined compressive strength of soils. In this context, a study was carried out to eliminate this deficiency in the literature and show the effect of reducing silty soils' compressive strength by using waste products.

One of the study's aims is to increase the unconfined compressive strength by mixing BA and RHA into silt soils. The ratios that provide the highest strength value were used in the literature studies in this context. Strength increases were measured by the unconfined compressive strength test, which has a simple experimental procedure, and it has been shown that this method, which can be performed in almost any soil laboratory, gives reliable results. The results obtained from the analyses can be listed as follows;

1. Although mixtures using ground 7% BA and 10% RHA caused a loss of strength in the short curing period, they provided a strength increase of 29.96% and 19.58%, respectively, in the long curing period.

2. Unmilled 10% RHA measured loss of strength at all curing times. The strength loss after 28 days of curing was measured as 29.70%.

3. In the samples where 7% BA + 10% RHA was used together, an increase in strength was detected at all curing periods. After the 28th day curing period, it achieved a strength increase of 91.66%.

As a result, it has been understood that BA and RHA increase strength when ground and used together. The high increase in strength in the 7% BA + 10% RHA mixture is attributed to the presence of CaO and SiO_2 in sufficient proportions. I recommend that future studies investigate the use of waste products together with alkalis.

Conflict of Interest

All authors certify that they have no affiliations with or involvement in any organization or entity with any financial interest or non-financial interest in the subject matter or materials discussed in this manuscript.

Ethics Committee Approval

Ethics committee approval is not required.

Author Contribution

Conceptization, methodology, laboratory analyzes, writing draft, proof reading and editing: MUY.

Acknowledgements

Not applicable

5. References

[1] Loveridge, N. (1999). Bone: more than a stick. Journal of animal science, 77(suppl_2), 190-196.

[2] Ifka, T., Palou, M. T., & Bazelova, Z. (2012). Influence of CaO and P 2 O 5 of bone ash upon the reactivity and the burnability of cement raw mixtures. Ceramics-Silikáty, 56(1), 76-84.

[3] Supraja, V., Raj, M. S., Nagarjuna, P. D., Vamsi, P., & Nagamani, V. A review paper on stabilization of red soil using rice husk ash..

[4] Gencel, O., Benli, A., Bayraktar, O. Y., Kaplan, G., Sutcu, M., & Elabade, W. A. T. (2021). Effect of waste marble powder and rice husk ash on the microstructural, physico-mechanical and transport properties of foam concretes exposed to high temperatures and freeze–thaw cycles. Construction and Building Materials, 291, 123374.

[5] Gencel, O., Sarı, A., Kaplan, G., Ustaoglu, A., Hekimoğlu, G., Bayraktar, O. Y., & Ozbakkaloglu, T. (2022). Properties of eco-friendly foam concrete containing PCM impregnated rice husk ash for thermal management of buildings. Journal of Building Engineering, 58, 104961.

[6] Ma, W., Wang, Y., Huang, L., Yan, L., & Kasal, B. (2023). Natural and recycled aggregate concrete containing rice husk ash as replacement of cement: Mechanical properties, microstructure, strength model and statistical analysis. Journal of Building Engineering, 66, 105917.

[7] Astm, D. (2010). 4318. Test Methods for Liquid Limit, Plastic Limit, and Plasticity Index of Soils, American Society for the Testing and Materials, ASTM Book of Standards Soil and Rock (I): D420–D5876, 4.

[8] Varol, D. (2006). Pirinç kabuğu külünden magnezyum silikat sentezi (Doctoral dissertation, Fen Bilimleri Enstitüsü).

[9] Akinniyi, D., & Ayininuola, M. G. (2018). Bone ash influence on soil consolidation. Malaysian Journal of Civil Engineering, 28(3).

[10] Shi, R. Y., Li, J. Y., Xu, R. K., & Qian, W. (2016). Ameliorating effects of individual and combined application of biomass ash, bone meal and alkaline slag on acid soils. Soil and Tillage Research, 162, 41-45.

[11] Kumar, V., Singh, A., & Garg, P. (2018). Stabilization of clayey soil using chicken bone ash. International Journal of Creative Research Thoughts, 6(2), 486-495.

[12] Brahmachary, T. K., Ahsan, M. K., & Rokonuzzaman, M. (2019). Impact of rice husk ash (RHA) and nylon fiber on the bearing capacity of organic soil. SN Applied sciences, 1(3), 273.

[13] Dewi, R., Borgan, W., Zunita, I., & Iqbal, M. M. (2019). Effect of deep soil mixing to increasing bearing capacity on peat soil. GEOMATE Journal, 17(63), 126-132.

[14] Aziz, M., Saleem, M., & Irfan, M. (2015). Engineering behaviour of expansive soils treated with rice husk ash [J]. Geomechanics and Engineering, 8(2), 173-186.

[15] Astm, D. (2023). 7012-23. Standard Test Methods for Compressive Strength and Elastic Moduli of Intact Rock Core Specimens under Varying States of Stress and Temperatures.

doi:10.55385/kastamonujes.1474468 KUJES 10(1): 29-37, 2024

Kastamonu University
Journal of Engineering and Sciences
e-ISSN 2667-8209
http://dergipark.gov.tr/kastamonujes

Possible Changes in Red Pine (*Pinus brutia* Ten.) Distribution Areas in Kastamonu due to Global Climate Change

Nihat Ertürk[a, *], **Burak Arıcak**[b]

[a] Department of Forest Engineering, Faculty of Forestry, Kastamonu University, Kastamonu, Türkiye
[b] Department of Forest Engineering, Faculty of Forestry, Bursa Technical University, Bursa, Türkiye
***Corresponding Author:** burak.aricak@btu.edu.tr

Received: **April 27, 2024** ◆ Accepted: **June 23, 2024** ◆ Published Online: **June 28, 2024**

Abstract: In this study, it was aimed to determine the current status of red pine (*Pinus brutia* Ten.) distribution areas in Kastamonu Forestry Regional Directorate, which is the Forestry Regional Directorate with the highest production in Türkiye, and the possible changes in suitable distribution areas due to global climate change. In the study, in addition to the current suitable distribution areas of red pine (*Pinus brutia* Ten.), suitable distribution areas in 2040, 2070 and 2100 according to SSP 126, SSP 370 and SSP 585 scenarios were determined. The results of the study show that there may be a loss of more than 15% (approximately 114,5 km^2) in the suitable distribution areas of red pine populations in Kastamonu until 2100 due to the effects of climate change. It does not seem possible for the species to adapt to these changes without human intervention. Therefore, it is recommended that necessary adjustments should be made in forest management plans taking into account the results of the study.

Keywords: Global climate change, *Pinus brutia* Ten., red pine, SSPs scenarios

Öz: Bu çalışmada, Türkiye'nin en fazla üretim yapılan Orman Bölge Müdürlüğü olan Kastamonu Orman Bölge Müdürlüğü'ndeki kızılçam (Pinus brutia Ten.) dağılım alanlarının mevcut durumunun ve uygun dağıtım alanlarında olası değişikliklerin belirlenmesi amaçlandı. küresel iklim değişikliği nedeniyle. Çalışmada kızılçamın (Pinus brutia Ten.) mevcut uygun yayılış alanlarının yanı sıra SSP 126, SSP 370 ve SSP 585 senaryolarına göre 2040, 2070 ve 2100 yıllarında uygun yayılış alanları belirlenmiştir. Araştırma sonuçları, Kastamonu'da kızılçam popülasyonlarının uygun yayılış alanlarında iklim değişikliğinin etkisiyle 2100 yılına kadar %15'ten fazla (yaklaşık 114,5 km2) kayıp olabileceğini göstermektedir. Türlerin insan müdahalesi olmadan bu değişimlere uyum sağlaması mümkün görünmüyor. Bu nedenle orman amenajman planlarında çalışmanın sonuçları dikkate alınarak gerekli düzenlemelerin yapılması önerilmektedir.

Anahtar Kelimeler: Küresel iklim değişikliği, *Pinus brutia* Ten., kızılçam, SSP senaryoları

1. Introduction

Climate is defined as the average weather conditions that remain the same over a wide area and over a very long time [1]. All phenotypic characters of living organisms are shaped under the influence of climate [2]. Therefore, changes in climatic parameters affect all living things directly or indirectly [3]. However, the living group most affected by climatic changes is plants, which have a limited migration mechanism [4]. It is often emphasized that the natural migration mechanism of plants cannot keep up with the speed of global climate change and therefore individual, population and species losses are inevitable [5]. It is stated that forest ecosystems will be the most affected by the global climate change process. Forests are the largest terrestrial carbon sink in the world and are the most effective and low-cost instruments that can be used to offset global greenhouse gas emissions. Therefore, the spatial loss of forest areas as a result of global climate change will further accelerate global climate change. Therefore, it is of great importance to determine the possible effects of global climate change especially on forests and to take the necessary measures, to provide the migration mechanism needed by plants by human hands, and to prevent species and population losses [6]. Due to the importance of the issue, many studies have been conducted on the change of suitable distribution areas of forest trees [1, 4-7].

However, these studies generally cover large areas and detailed studies are needed to plan appropriate silvicultural interventions. In this study, it was aimed to determine in detail how the suitable distribution areas of red pine (*Pinus brutia* Ten.) may change due to global climate change in Kastamonu Regional Forest Directorate, which is the Regional Forest Directorate with the highest wood raw material production in Türkiye. Unlike similar studies, the current distribution areas of the species were also evaluated within the scope of the study.

2. Material and Method

The study was conducted to model the changes in the potential distribution areas of red pine (*Pinus brutia* Ten.), one of the most important tree species for Türkiye and the Mediterranean basin, in Kastamonu due to global climate change. Within the scope of the study, firstly the current distribution area of the species subject to the study, then the current potential distribution area was determined. In the next stage, the potential distribution areas of the species in Kastamonu in 2040, 2070 and 2100 were tried to be determined. MaxEnt 3.4.1 software was used for modeling the potential distribution areas of the species and ArcGIS 10.5 software was used for map representation. In this study, 19 bioclimatic variables were used, which are the most frequently used variables in similar studies [7, 8]. The biological variables used in the study are given in Table 1.

Table 1. Bioclimatic variables used in modelling

Codes	Bioclimatic variables	Unit
Bio1	Annual Mean Temperature	°C
Bio2	Mean Diurnal Range (Mean of monthly [max temp - min temp])	°C
Bio3	Isothermality (Bio2/Bio7) (* 100)	-
Bio4	Temperature Seasonality (standard deviation *100)	(coeff. of variation °C)
Bio5	Max Temperature of Warmest Month	°C
Bio6	Min Temperature of Coldest Month	°C
Bio7	Temperature Annual Range (Bio5-Bio6)	°C
Bio8	Mean Temperature of Wettest Quarter	°C
Bio9	Mean Temperature of Driest Quarter	°C
Bio10	Mean Temperature of Warmest Quarter	°C
Bio11	Mean Temperature of Coldest Quarter	°C
Bio12	Annual Precipitation	mm
Bio13	Precipitation of Wettest Month	mm
Bio14	Precipitation of Driest Month	mm
Bio15	Precipitation Seasonality (coefficient of variation)	percent
Bio16	Precipitation of Wettest Quarter	mm
Bio17	Precipitation of Driest Quarter	mm
Bio18	Precipitation of Warmest Quarter	mm
Bio19	Precipitation of Coldest Quarter	mm
Q	Emberger climate classification	-

Socio-economic pathways (SSPs) include five main SPPs (SSP 119, SSP 126, SSP 245, SSP 370, SSP 585). In this study, SSP 126, SSP 370 and SSP 585 scenarios were used. These scenarios and the method used in the study are among the methods and scenarios frequently used in similar studies [5, 10].

3. Findings

The validation values of the training data and test data in the ROC curve obtained as a result of the modeling performed within the scope of the study were determined as 0.960 (AUC>0.5). These findings show that the model has a very high predictive power (Figure 1).

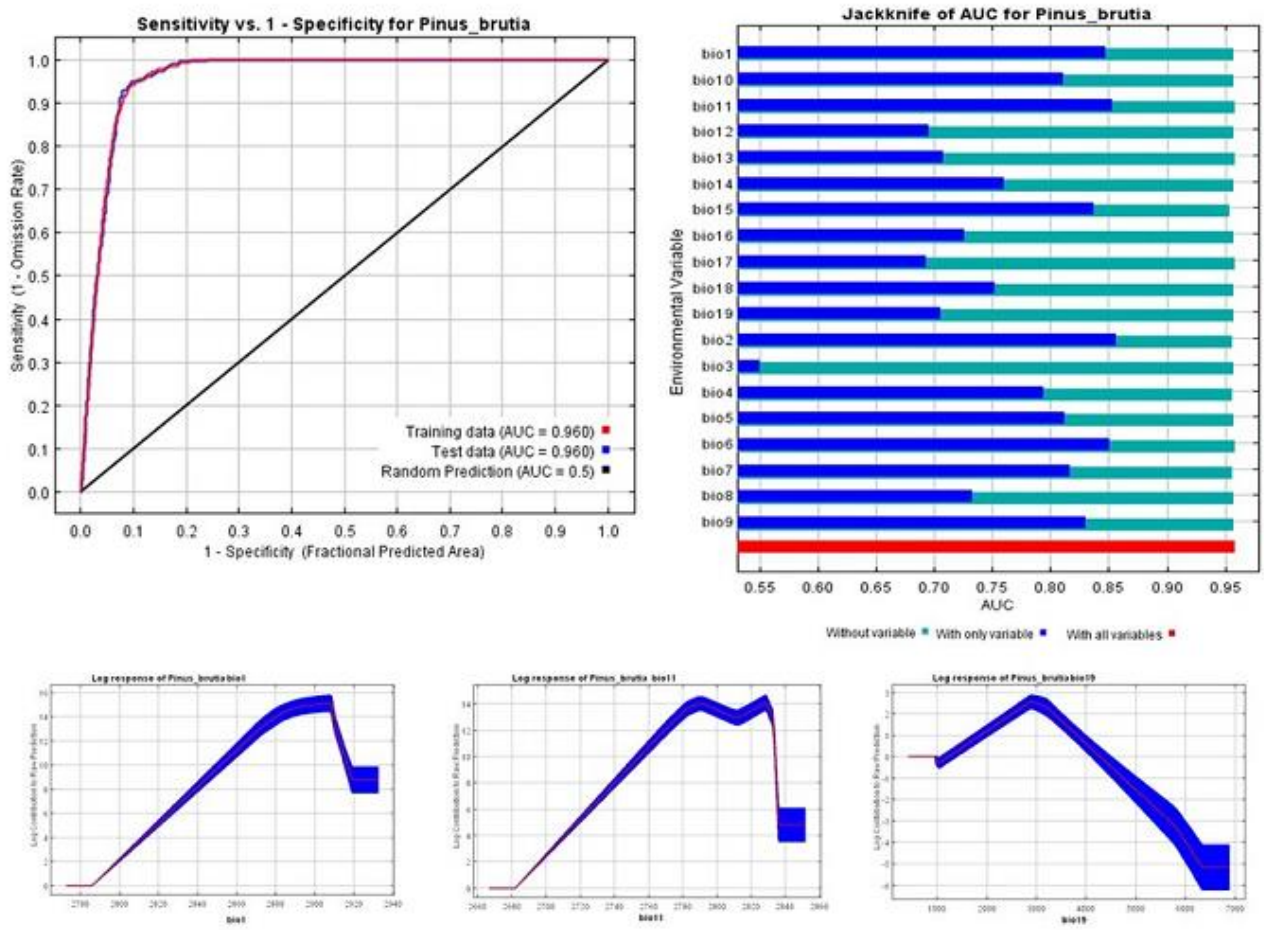

Figure 1. Effects of environmental factors on the distribution area of *Pinus brutia*

According to the gain table created for *Pinus brutia* with the Jacknife option in the model, the environmental variables that individually affect the distribution of the species in the training data at the highest level are determined as the average daily range (temperature range) [Bio2], the minimum temperature of the coldest month [Bio6] and the average temperature of the coldest quarter (3 months) [Bio11]. This reveals that the species is significantly affected by temperature. The current distribution areas of *Pinus brutia*, suitable distribution areas according to the model and distribution areas depending on global climate change are shown in Figure 2.

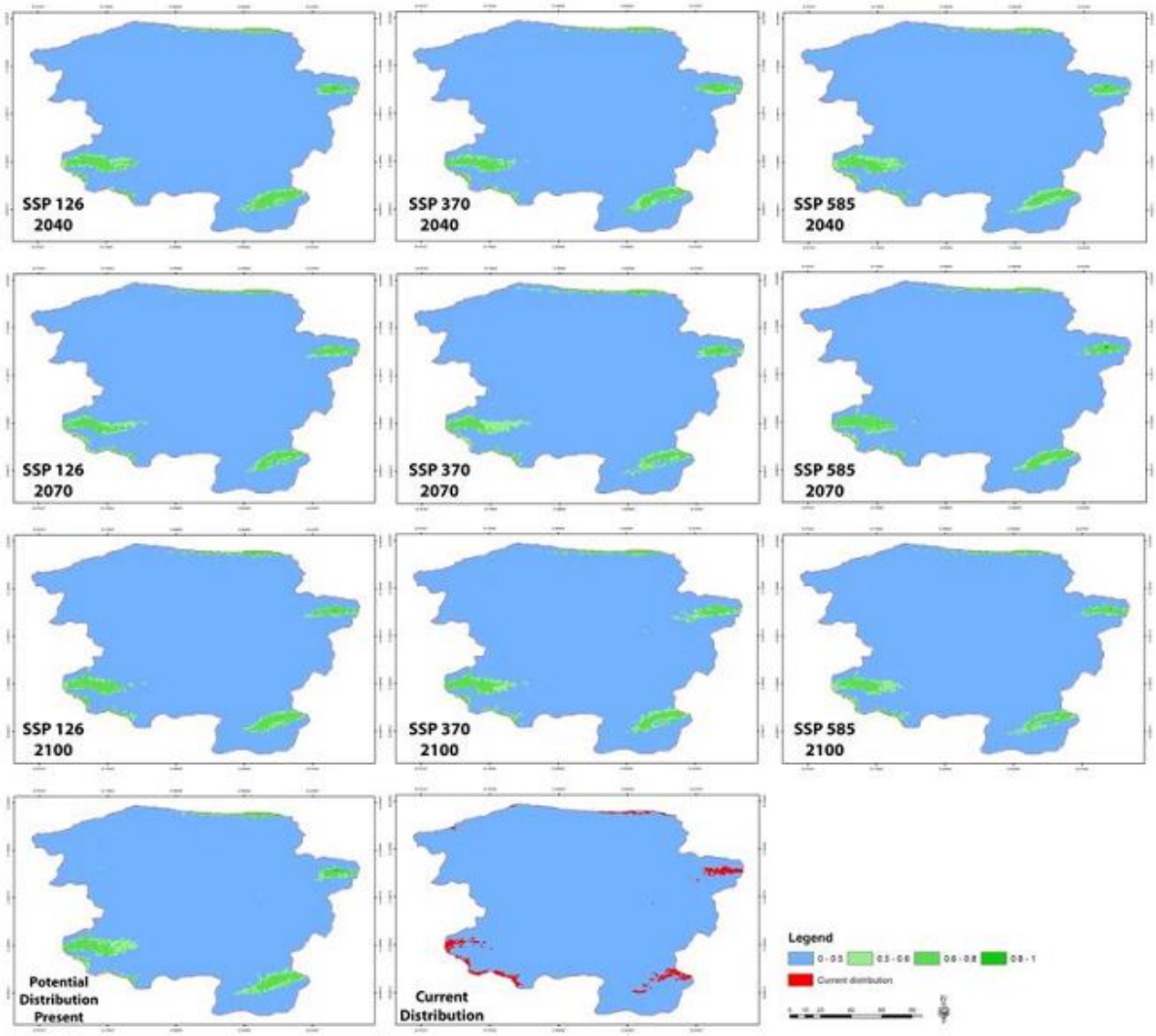

Figure 2. Suitable distribution areas of *Pinus brutia* depending on global climate change

When the current distribution areas of *Pinus brutia* are examined, it is seen that the distribution areas of *Pinus brutia* are located in the north of the province near the sea, in Hanönü district in the northeast, in Tosya district in the southeast and in Araç district in the southwest. These distribution areas are the regions where the altitude is quite low in Kastamonu. When the current suitable distribution areas of *P. brutia* are compared with the current distribution areas, it is seen that they are largely compatible. It was determined that the suitable distribution areas of the species are mostly in a narrow area in Tosya, Hanönü and Araç districts and on the coastline, as in the current distribution areas, and that there are local suitable distribution areas in very small areas. Apart from this, it can be said that there will be losses and gains in the suitable distribution areas of the species in general, but losses will definitely be seen in suitable distribution areas until 2100. According to the SSP 126 scenario, the rate of change in the suitable distribution areas of P. brutia in 2040, 2070 and 2100 compared to today is given in Table 2.

Table 2. Change of suitable distribution areas (km^2) of *P. brutia* according to SSP 126 scenario

Compliance	2020 available	2020 potential	SSPS 126		
			2040	2070	2100
0-0.5	12876	12317	12347.2	12410.9	12392.3
0.5-0.6		298.7	232.4	224.1	188.6
0.6-0.8	176.2	430.7	470.7	415.9	468.1
0.8-1		5.8	1.9	1.3	3.2
Total (km^2)	13052.2	13052.2	13052.2	13052.2	13052.2

When the table values are analyzed, it is calculated that *P. brutia* has a total potential distribution area of 735.2 km^2, of which 298.7 km^2 is suitable, 430.7 km^2 is highly suitable and 5.8 km^2 is very suitable, whereas the current *P. brutia* distribution area is 176.2 km^2. According to the SSP 126 scenario, when the change in the suitable distribution areas of *P. brutia* in the near future is analyzed, it is estimated that there will be a decrease in the total suitable distribution area until 2100, and there will be some increase in 2100, but this amount will still be lower than today. While the suitable distribution area of *P. brutia* is 298.7 km2 today, it is predicted to be 232.4 km^2 in 2040, 224.1 km^2 in 2070 and 188.6 km^2 in 2100.

The highly suitable distribution areas, which are 430.7 km^2 today, are estimated to be 470.7 km^2 in 2040, 415.9 km^2 in 2070 and 468.1 km^2 in 2100. The very suitable distribution areas, which are 5.8 km^2 today, are estimated to be 1.9 km^2 in 2040, 1.3 km^2 in 2070 and 3.2 km^2 in 2100. Therefore, the total area of suitable distribution area, which is 735.2 km^2 today, is projected to increase to 705.0 km^2 in 2040, 641.3 km^2 in 2070 and 659.9 km^2 in 2100 in the SSP 126 scenario. In these figures, it is noteworthy that, unlike other species in general, the amount of highly suitable distribution areas is higher than the amount of suitable distribution areas. According to the SSP 370 scenario, the rate of change in the suitable distribution areas of *P. brutia* compared to the present day is given in Table 3.

Table 3. Change of suitable distribution areas (km^2) of *P. brutia* according to SSP 370 scenario

Compliance	2020 available	2020 potential	SSPS 370		
			2040	2070	2100
0-0.5	12876	12317	12386.5	12368.4	12324.7
0.5-0.6		298.7	217.0	320.6	280.7
0.6-0.8	176.2	430.7	445.5	360.6	446.2
0.8-1		5.8	3.2	2.6	0.6
Total (km^2)	13052.2	13052.2	13052.2	13052.2	13052.2

According to the SSP 370 scenario, the total area of suitable distribution of *P. brutia* is expected to decrease in 2040 compared to today, but increase in 2070 compared to 2040 and in 2100 compared to 2070. However, these increases will not compensate for the losses until 2040. According to the calculations, according to the SSP 370 scenario, the area of suitable distribution, which is 298.7 km^2 today, will be 217.0 km^2 in 2040, 320.6 km^2 in 2070 and 280.7 km^2 in 2100. The highly suitable distribution areas, which are approximately 430.7 km^2 today, are estimated to be 445.5 km^2 in 2040, 360.6 km^2 in 2070 and 446.2 km^2 in 2100. On the other hand, it is estimated that the very suitable distribution areas will decrease from 5.8 km^2 today to 3.2 km^2 in 2040, 2.6 km^2 in 2070 and 0.6 km^2 in 2100. Therefore, according to the SSP 370 scenario, the total suitable distribution area, which is 735.2 km^2 today, is projected to be 665.7 km^2 in 2040, 683.8 km^2 in 2070 and 727.5 km^2 in 2100. According to the SSP 585 scenario, the rate of change of the suitable distribution areas of *P. brutia* compared to the present day is given in Table 4.

Table 4. Change of suitable distribution areas (km^2) of *P. brutia* according to SSP 585 scenario

Compliance	2020 available	2020 potential	SSPS 585		
			2040	2070	2100
0-0.5	12876	12317.0	12354.9	12410.9	12431.5
0.5-0.6		298.7	273.6	190.6	252.4
0.6-0.8	176.2	430.7	421.1	446.2	366.4
0.8-1		5.8	2.6	4.5	1.9
Total (km^2)	13052.2	13052.2	13052.2	13052.2	13052.2

When the table showing the change in the suitable distribution areas of *P. brutia* according to the SSP 585 scenario is analyzed, it can be said that the total suitable distribution area will decrease significantly in 2040 compared to the present day, will increase in 2070 compared to 2040, and this increase will continue until 2100. According to the calculations made, it is estimated that the area of suitable distribution, which is 298.7 km2 today, will be 273.6 km^2 in 2040, 190.6 km^2 in 2070 and 252.4 km^2 in 2100 according to the SSP 585 scenario. The highly suitable distribution areas, which are approximately 430.7 km^2 today, are estimated to be 421.1 km^2 in 2040, 446.2 km^2 in 2070 and 366.4 km^2 in 2100. It is predicted that the areas of very suitable distribution will decrease from 5.8 km^2 today to 2.6 km^2 in 2040, increase again to 4.5 km^2 in 2070 and decrease again to 1.9 km^2 in 2100. Therefore, the total suitable distribution area, which is 735.2 km2 today, is estimated to be 697.3 km^2 in 2040, 641.3 km^2 in 2070 and 620.7 km^2 in 2100 according to the SSP 585 scenario.

4. Discussion and Conclusion

The results of the study show that the suitable distribution areas of red pine populations in Kastamonu will change due to the effects of climate change. According to the calculations made, the amount of suitable distribution area in Kastamonu, which is currently 735.2 km^2, will decrease to 659.9 km^2 according to the SSP 126 scenario, 727.5 km^2 according to the SSP 370 scenario and 620.7 km^2 according to the SSP 585 scenario by 2100. Therefore, it is estimated that the amount of suitable distribution areas of the species in Kastamonu may be lost by more than 15% by 2100. In the studies conducted, it is estimated that different species will be affected by global climate change at different levels. For example, the total suitable distribution area of fir (*Abies bornmülleriana*) in Kastamonu, which is 2968.8 km^2 today, is estimated to be 3106.6 km2 in 2040, 3194.8 km^2 in 2070 and 3179.4 km^2 in 2100 according to the SSP 585 scenario [5]. Again in Kastamonu, the total suitable distribution area of beech, which is 3454.8 km^2 today, is estimated to be 3540.6 km^2 in 2040, 3648.7 km^2 in 2070 and 3622.3 km^2 in 2100 according to the SSP 585 scenario [5]. According to the SSP 585 scenario, the total area of chestnut (*Castanea sativa*) suitable distribution in Kastamonu, which is 868.6 km^2 today, is estimated to be 798.3 km^2 in 2040, 815.1 km^2 in 2070 and 800.9 km^2 in 2100 [10]. Therefore, according to the SSP 585 scenario in Kastamonu, it is predicted that there will be an increase in the total suitable distribution areas of fir and beech until 2100, but there will be significant losses in the suitable distribution areas of chestnut. It is stated that chestnut is the species most at risk among these species and that chestnut suitable distribution areas may disappear completely by 2100 [9]. Possible changes of different species have also been evaluated in studies conducted throughout Türkiye. In one study, according to the SSSP 245 scenario, the suitable distribution areas of A. bornmuelleriana are predicted to decrease in the coming years, especially at altitudes above 1400 m, whereas there will be a general increase at altitudes of 200-600 m [1]. According to another study, the distribution areas of Tilia cordata in western Marmara will almost completely disappear, while the distribution areas of Tilia tomentosa in southern Anatolia and the Black Sea region will decrease significantly [8]. It is stated that the distribution areas of Fraxinus excelsior L may decrease by 7.58% by 2100 [10]. It is estimated that Carpinus betulus may experience population losses exceeding 25% at altitudes below 1600 m and Carpinus orientalis may experience population losses exceeding 30% at altitudes below 1000 m [11]. Similarly, the Quercus libani suitable distribution area, which is currently 72,819 km^2 in Türkiye, is predicted to decrease to 63,390 km^2 by 2070 [12].

Türkiye is among the "countries at risk" and highly vulnerable to climate change, and future climate projections indicate that by 2100, Türkiye's annual temperature will increase across the entire country, especially in the Aegean region, where temperature increases can reach up to 6 ºC [7]. The Mediterranean region is dominated by red pine, and red pine is one of the species that will be most affected by this process. As a matter of fact, in a study, it is stated that while the ratio of the geographical distribution of *P. pinea* to the geographical area of Türkiye is 16.08% today, this ratio may decrease to 2.28% in 2070, that is, the loss of its potential distribution area may approach 85% [13]. Studies conducted in different parts of the world also indicate that some species may experience great losses in their suitable distribution areas. It is estimated that the reduction in the potential distribution area of F. sylvatica in Europe could reach 56% [14], the loss of habitat for different species in mountainous areas in Mexico could reach 46-77% by 2060 [15], and Pinus armandii suitable habitat in the Hengduan Mountains of China will gradually disappear [16].

Global climate change is considered as a process that will lead to significant changes in climate parameters. Because all phenotypic characters of living organisms are shaped by their genetic structure [17, 18] and environmental factors [19, 20]. Climate is one of the most important environmental factors [21, 22]. It is stated that changes in climatic parameters, i.e. global climate change, will directly or indirectly affect forests by increasing the spread of insects and fungi [23], forest fires [24], alien species invasions [1], affecting water and nutrient availability, precipitation regime [11]. It is emphasized that the most important effects of the global climate change process will be temperature increase and decrease in water resources [25, 26]. In addition, increased UV-B rays [27] and radiation will cause significant stress in plants [28]. Studies have estimated that the northern half of Türkiye will experience a much larger decrease in summer precipitation than the southern half [9]. It is stated that the increase in temperature and decrease in precipitation in cities such as Samsun [29], Düzce [30], Kastamonu [31], Düzce [32] which are located in the northern half of Türkiye, may cause aridification in the climate to occur very rapidly.

As a result, global climate change is a process that can directly or indirectly affect all living things and ecosystems on earth and is defined as one of the two irreversible problems that the world has to cope with [33, 34]. The living group that will be most affected by this process is plants, which do not have an effective mobility. Since the life on earth is directly or indirectly dependent on plants [35-39], it is inevitable that all living things in the world will be affected by global climate change.

5. Recommendations

The results of the study show that there will be significant changes in the distribution areas of the red pine populations in Kastamonu and that the loss of suitable distribution area may exceed 15% by 2100. It does not seem possible for the species to adapt to these changes without human intervention. Therefore, it is recommended that necessary adjustments be made in forest management plans taking into account the results of the study.

Global climate change is defined as an irreversible problem. Therefore, it is of great importance to take measures to ensure that plants are minimally affected by the effects of global climate change. Reducing the impact of this process in forests and minimizing species and population losses is possible by predicting the possible future changes from today and taking measures and planning according to the changes that may occur. The fact that this process has different effects on forests means that species need different silvicultural interventions. Which silvicultural interventions will provide the greatest benefit for which species should be determined depending on the ecological context of the forest and the adaptability of the species. Current silvicultural practices should therefore be reviewed and redesigned to take into account the impacts of global climate change.

Conflict of Interest

All authors certify that they have no affiliations with or involvement in any organization or entity with any financial interest or non-financial interest in the subject matter or materials discussed in this manuscript.

Ethics Committee Approval

Ethics committee approval is not required.

Author Contribution

Conceptization: BC, GS; methodology and laboratory analyzes: BC, GS; writing draft: BC, GS; proof reading and editing: Other: All authors have read and agreed to the published version of manuscript.

Acknowledgements

This research is Nihat ERTÜRK's PhD Thesis in Kastamonu University, Institute of Science, Programs of Forest Engineering conducted one of part of this research. We sincerely thanks to Kastamonu University Institute of Science.

6. References

[1] Tekin, O., Cetin, M., Varol, T., Ozel, H. B., Sevik, H., & Zeren Cetin, I. (2022). Altitudinal migration of species of Fir (Abies spp.) in adaptation to climate change. Water, Air, & Soil Pollution, 233(9), 1-16.

[2] Sevik, H., Çetin, M., & Kapucu, O. (2016). Effect of light on young structures of Turkish fir (Abies nordmanniana subsp. bornmulleriana). Oxidation Communications, 39(1), 485-492.

[3] Işınkaralar, Ö. (2024). Spatio-temporal change of the morphology in west corridor development region of Ankara city and 2022-2039 growth estimation. Megaron, 19(1).

[4] Varol, T., Cetin, M., Ozel, H. B., Sevik, H., Zeren Cetin, I. (2022a). The effects of climate change scenarios on Carpinus betulus and Carpinus orientalis in Europe. Water, Air and Soil Pollution, 233, 45.

[5] Ertürk, N., Arıcak, B., Yiğit, N., & Sevik, H. (2024). Potential Changes in the Suitable Distribution Areas of Fagus orientalis Lipsky in Kastamonu Due to Global Climate Change. Forestist, 74(2).

[6] Erturk, N., Aricak, B., Sevik, H., & Yigit, N. (2024). Possible Change in Distribution Areas of Abies in Kastamonu due to Global Climate Change. Kastamonu University Journal of Forestry Faculty, 24 (1), 81-91.

[7] Varol, T., Canturk, U., Cetin, M., Ozel, H. B., Sevik, H., & Zeren Cetin, I. (2022b). Identifying the suitable habitats for Anatolian boxwood (Buxus sempervirens L.) for the future regarding the climate change. Theoretical and Applied Climatology, 150(1), 637-647.

[8] Isinkaralar, O., Świsłowski, P., Isinkaralar, K., & Rajfur, M. (2024). Moss as a passive biomonitoring tool for the atmospheric deposition and spatial distribution pattern of toxic metals in an industrial city. Environmental Monitoring and Assessment, 196(6), 513.

[9] Cobanoglu, H., Canturk, U., Koç, İ., Kulaç, Ş., & Sevik, H. (2023). Climate change effect on potential distribution of anatolian chestnut (Castanea sativa Mill.) in the upcoming century in Türkiye. Forestist, 73(3), 247-256

[10] Erturk N., & Arıcak, B. (2024). Potential change of chestnut (Castanea sativa Mill.) distribution areas in Kastamonu due to global climate change, World Journal of Advanced Research and Reviews (In Press)

[11] Varol, T., Canturk, U., Cetin, M., Ozel, H. B., Sevik, H. (2021a). Impacts of climate change scenarios on European ash tree (Fraxinus excelsior L.) in Turkey. Forest Ecology and Management. Forest Ecology and Management, 491(2021b),119199.

[12] Çoban, H. O., Örücü, Ö. K., & Arslan, E. S. (2020). MaxEnt modeling for predicting the current and future potential geographical distribution of Quercus libani Olivier. Sustainability, 127, 2671.

[13] Akyol, A., & Örücü, Ö. K. (2020). Investigation and evaluation of stone pine Pinus pinea L. current and future potential distribution under climate change in Turkey. Cerne, 25, 415-423.

[14] Thurm, E. A., Hernandez, L., Baltensweiler, A., Ayan, S., Rasztovits, E., Bielak, K., Zlatanov, T. M., Hladnik, D., Balic, B., Freudenschuss, A., Büchsenmeister, R., & Falk, W. (2018). Alternative tree species under climate warming in managed European forests. Forest Ecology and Management, 430, 485–497.

[15] Gómez-Pineda, E., Blanco-García, A., Lindig-Cisneros, R., O'Neill, G. A., Lopez-Toledo, L., & Sáenz-Romero, C. (2021). Pinus pseudostrobus assisted migration trial with rain exclusion: Maintaining Monarch Butterfly Biosphere Reserve forest cover in an environment affected by climate change. New Forests, 52(6), 995–1010.

[16] Ning, H., Ling, L., Sun, X., Kang, X., & Chen, H. (2021). Predicting the future redistribution of Chinese white pine Pinus armandii Franch. Under climate change scenarios in China using species distribution models. Global Ecology and Conservation, 25, e01420.

[17] Hrivnák, M., Krajmerová, D., Paule, L., Zhelev, P., Sevik, H., Ivanković, M., ... & Gömöry, D. (2023). Are there hybrid zones in Fagus sylvatica L. sensu lato?. European Journal of Forest Research, 1-14.

[18] Sulhan, O. F., Sevik, H., & Isinkaralar, K. (2023). Assessment of Cr and Zn deposition on Picea pungens Engelm. in urban air of Ankara, Türkiye. Environment, development and sustainability, 25(5), 4365-4384.

[19] Özel, H. B., Şevik, H., Yıldız, Y., & Çobanoğlu, H. (2024). Effects of Silver Nanoparticles on Germination and Seedling Characteristics of Oriental Beech (Fagus orientalis) Seeds. BioResources, 19(2). 2135-2148.

[20] Koç, İ., Canturk, U., Isinkaralar, K., Ozel, H. B., & Sevik, H. (2024). Assessment of metals (Ni, Ba) deposition in plant types and their organs at Mersin City, Türkiye. Environmental Monitoring and Assessment, 196(3), 282.

[21] Işınkaralar, O., Işınkaralar, K., Sevik, H., Kucuk, O. (2023). Bio-climatic Comfort and Climate Change Nexus: A Case Study in Burdur Basin. Kastamonu University Journal of Forestry Faculty, 23(3), 241-249. https://doi.org/10.17475/kastorman.1394916

[22] Isinkaralar, K. (2022). Some atmospheric trace metals deposition in selected trees as a possible biomonitor. Romanian Biotechnological Letters, 27(1), 3227-3236.

[23] Toczydlowski, A. J., Slesak, R. A., Kolka, R. K., & Venterea, R. T. (2020). Temperature and water-level effects on greenhouse gas fluxes from black ash (Fraxinus nigra) wetland soils in the Upper Great Lakes region, USA. Applied Soil Ecology, 153, 103565.

[24] Ertugrul, M., Ozel, H. B., Varol, T., Cetin, M., & Sevik, H. (2019). Investigation of the relationship between burned areas and climate factors in large forest fires in the Çanakkale region. Environmental monitoring and assessment, 191, 1-12.

[25] Cetin, M., Sevik, H., Koc, I., & Cetin, I. Z. (2023). The change in biocomfort zones in the area of Muğla province in near future due to the global climate change scenarios. Journal of Thermal Biology, 112, 103434.

[26] Isinkaralar, O., Isinkaralar, K., Sevik, H., & Küçük, Ö. (2024). Spatial modeling the climate change risk of river basins via climate classification: a scenario-based prediction approach for Türkiye. Natural Hazards, 120(1), 511-528.

[27] Ozel, H. B., Abo Aisha, A. E. S., Cetin, M., Sevik, H., & Zeren Cetin, I. (2021a). The effects of increased exposure time to UV-B radiation on germination and seedling development of Anatolian black pine seeds. Environmental Monitoring and Assessment, 193, 388.

[28] Ozel, H. B., Cetin, M., Sevik, H., Varol, T., Isik, B., & Yaman, B. (2021b). The effects of base station as an electromagnetic radiation source on flower and cone yield and germination percentage in Pinus brutia Ten. Biologia Futura, 72, 359-365.

[29] Koç, İ. (2022). Determining the near-future biocomfort zones in Samsun province by the global climate change scenarios. Kastamonu University Journal of Forestry Faculty, 22(2), 181-192.

[30] Koç, İ. (2021). Changes that may occur in temperature, rain, and climate types due to global climate change: the example of Düzce. Turkish Journal of Agriculture-Food Science and Technology, 9(8), 1545-1554.

[31] Gur, E., Palta, Ş., Ozel, H. B., Varol, T., Sevik, H., Cetin, M., & Kocan, N. (2024). Assessment of Climate Change Impact on Highland Areas in Kastamonu, Turkey. Anthropocene, 100432.

[32] Koç, İ. (2021). Küresel iklim değişikliğinin Bolu'da bazı iklim parametreleri ve iklim tiplerine etkisi. Bartın Orman Fakültesi Dergisi, 23(2), 706-719.

[33] Yayla, E. E., Sevik, H., & Isinkaralar, K. (2022). Detection of landscape species as a low-cost biomonitoring study: Cr, Mn, and Zn pollution in an urban air quality. Environmental Monitoring and Assessment, 194(10), 1-10.

[34] Key, K., Kulaç, Ş., Koç, İ., & Sevik, H. (2022). Determining the 180-year change of Cd, Fe, and Al concentrations in the air by using annual rings of Corylus colurna L. Water, Air, & Soil Pollution, 233(7), 244.

[35] Yigit, N., Mutevelli, Z., Sevik, H., Onat, S.M., Ozel, H.B., Cetin, M., Olgun, C. (2021). Identification of Some Fiber Characteristics in Rosa sp. and Nerium oleander L. Wood Grown under Different Ecological Conditions. BioResources, 16(3): 5862-5874.

[36] Ghoma, W. E. O., Sevik, H., & Isinkaralar, K. (2023). Comparison of the rate of certain trace metals accumulation in indoor plants for smoking and non-smoking areas. Environmental science and pollution research, 30(30), 75768-75776.

[37] Koç, İ., & Nzokou, P. (2023). Combined effects of water stress and fertilization on the morphology and gas exchange parameters of 3-year-old Abies fraseri (Pursh) Poir. Acta physiologiae plantarum, 45(3), 49.

[38] Sevik, H., Yildiz, Y., Ozel, H.B. (2024). Phytoremediation and Long-term Metal Uptake Monitoring of Silver, Selenium, Antimony, and Thallium by Black Pine (Pinus nigra Arnold), BioResources, 19(3). 4824-4837.

[39] Koç, İ., Nzokou, P., & Cregg, B. (2022). Biomass allocation and nutrient use efficiency in response to water stress: Insight from experimental manipulation of balsam fir, concolor fir and white pine transplants. New Forests, 53(5), 915-933.

doi:10.55385/kastamonujes.1477345 KUJES 10(1):38-43, 2024

Kastamonu University
Journal of Engineering and Sciences
e-ISSN 2667-8209
http://dergipark.gov.tr/kastamonujes

Reduced Graphene Synthesis via Eco-Friendly Electrochemical Exfoliation Method

Gülbahar Bilgiç Tüzemen

Department of Metallurgy and Material Engineering, Faculty of Engineering-Architecture, Nevşehir Hacı Bektaş Veli University, Nevşehir, Türkiye
Corresponding Author: glbhrblg@nevsehir.edu.tr

Received: **May 2, 2024** ◆ Accepted: **June 14, 2024** ◆ Published Online: **June 28, 2024**

Abstract: A novel approach to mass producing graphene without inadvertent damage was needed to meet the increasing demand for the material. Graphite electrochemical exfoliation (EE) is an intriguing method for the large-scale, quick, and easy manufacture of graphene. Using leftover whey as an electrolyte, the EE of commercial graphite was examined in this work. It was shown that a straightforward and affordable exfoliation technique may produce graphene that, in the absence of functionalization or surfactant, forms a stable dispersion in the waste solvent. Because wastewater is acidic, it has been shown that storing it at +4 degrees aids EE. X-ray diffraction (XRD) was used to satisfactorily validate the manufactured graphene's existence. The results point to a low-cost method of producing graphene and graphene oxide.

Keywords: Graphene, waste cheese water, electrochemical exfoliation

Öz: Grafene yönelik artan talep, gereksiz hasara yol açmadan seri üretime geçmenin yeni bir yolunu gerektiriyordu. Bu yüzden grafitin pul pul dökülmesi basit, hızlı ve büyük ölçekli grafen üretimi için ilginç bir yaklaşımdır. Bu çalışmada atık peynir altı suyu elektrolit olarak kullanılarak ticari grafitin elektrokimysal pul pul dökülmesi araştırıldı. İşlevselleştirme ve yüzey aktif madde olmadan atık çözücü içinde stabil bir dağılım oluşturan grafen hazırlamak için basit ve uygun maliyetli bir elektrokimysal pul pul dökülme yöntemi gösterilmiştir. +4 derecede depolanan atık suyun asidik yapısından dolayı elektrokimyasal pul pul dökülmeye yardımcı olduğu gözlemlenmiştir. Üretilen grafenin varlığı X-ışını kırınımı (XRD) ile başarıyla doğrulandı. Bulgular, grafen ve grafen oksidin sentezlenmesi için düşük maliyetli bir üretim süreci önermektedir.

Anahtar Kelimeler: Grafen, atık peynir suyu, elektrokimyasal pul pul dökülme

1. Introduction

Graphene is a planar sheet one atom thick, composed of hexagon-shaped carbon atoms from sp^2 hybridization. Its mechanical, thermal, optical, and electrical qualities are outstanding. Moreover, graphene acts as a semimetal and has a zero-band gap due to its two-dimensional structure [1]. Graphene may be produced by several methods, such as ultrahigh vacuum annealing of single crystal SiC, mechanical or electrochemical exfoliation and cleavage, and chemical vapor deposition [2-4]. A low-cost, environmentally friendly technique for producing high-yield graphene is EE of graphite, which yields one-atom-thick graphene with desired features. It has long been recognized that graphite and other species may combine to make helpful intercalation compounds, or graphite intercalation compounds, which are frequently created electrochemically. Researchers have expanded GIC chemistry to electrochemically exfoliate graphene from natural graphite in light of the recent discovery of graphene [2, 3]. One of the increasing number of methods for producing graphene is electrochemical exfoliation. Wet chemical exfoliation techniques, like the modified Hummers process used to make graphene oxide, are connected to the electrochemical approach. However, unlike conventional techniques, which frequently rely on strong oxidants, electrochemical techniques use the conductive qualities of graphite to intercalate molecules between graphene layers. Much work has been done recently on the easy, quick, affordable, and environmentally acceptable EE of graphite to produce high-grade graphene [5]. Comparing this procedure to other conventional methods, it appears promising for manufacturing huge amounts of graphene [2]. Moreover, functionalized graphene might be produced by the exfoliation process. During the procedure, some factors need to be controlled, including the number of probes, the amount of current utilized, and the chemicals employed. The methods are similar in that an electrolyte (aqueous or nonaqueous solution, for example) and an electric current are often used to induce structural expansion in a graphite electrode [2]. Depending on the charge of the intermediate ions, the graphite electrode can operate as an anode or cathode and exhibit oxidation or reduction processes, respectively.

A positive or negative charge can be applied to the material by employing graphite as an electrode, which promotes the intercalation of oppositely charged ions and facilitates exfoliation. The electrochemical process is promising for

producing graphene in large quantities and may offer several benefits over conventional chemical approaches [5]. An example of a wet chemical procedure that can be less expensive for mass manufacturing is the electrochemical approach, which is similar to mechanical exfoliation, molecular assembly, and chemical vapor deposition (CVD). Even more than this, by using electrochemical activation instead of harsh chemicals, electrochemical manufacturing may be able to achieve a simpler stage in the purification of the final product. Electrochemically generated graphene can have a controllable degree of oxidation and low-hole flaws, making it a reasonably high-quality material. Electrochemically produced graphene is expected to have industrial uses in energy storage, electronics, coatings, and nanocomposites in other words, it will be used in all of the applications that have been proposed for graphene [5-14]. Although many methods have been proposed as successful in generating graphene, no one has yet discovered a flawless method that produces graphene without any flaws. As previously mentioned, compared to other methods, EE is a simple, rapid, and inexpensive process to produce graphene. Enough high-quality graphene materials need to be developed to satisfy the requirements of all these technological applications. During the EE process, when direct current is applied to two electrode arrays, strong particles are formed at both electrodes, and the anodic graphite and electrolyte begin to separate [6]. Unlike other peeling techniques, this approach requires no equipment and usually requires natural light. Furthermore, it is less harmful than other chemical methods that include potentially hazardous solvents or reagents [6, 7].

A straightforward and efficient method for producing graphene involves electrochemically exfoliating graphite rods in acidic liquids, as suggested by Coroş, M. and associates [11]. The graphene oxide peak diminishes or even vanishes when the EE trend is reduced from +6 to +2.5 V, according to the nanosheets' XRD patterns. It has been shown that by varying the applied voltage, graphene with varying degrees of oxidation may be generated. At a bias of +3 V, an ideal graphene sample was made in an H_2SO_4:HNO_3 combination.

The simple synthesis of graphene by electro-exfoliation employing several oxidizing agents (HNO_3, $NaNO_3$, H_2SO_4, and H_2O_2) in the presence of sodium dodecyl benzenesulfonate as a surfactant was proven by A.A.B. Hamra and colleagues [12]. The EE of graphite rods was dramatically altered by several surfactant-oxidizing agent solutions at varied concentrations. Moreover, graphene is directly generated via vacuum filtration and used as a supercapacitor electrode. The impact of electrolyte type on capacitance performance was examined using nylon membrane and polymer gel, both of which contained 2.0 M potassium hydroxide. The polymer gel electrolyte demonstrated an astounding capacity retention rate of more than 100% after 1000 charge/discharge cycles, whereas the nylon membrane electrolyte recorded a capacity retention rate of just 94%. The manufactured supercapacitor's capacity to light a light-emitting diode while charging reveals its promise for practical uses.

The EE of two distinct graphite predecessors at an applied direct current voltage of +12 V was shown by Marković et al [13]. The results of the characterization methods (X-ray diffraction, X-photoelectron spectroscopy, etc.) indicated that the exfoliated powder is highly functionalized and resembles graphene oxide in terms of its low carbon/oxygen concentration. After being disseminated in N,N′-dimethylformamide, the exfoliated graphene sheets were vacuum-filtered onto ano-discs and then moved to glass-ceramic substrates.

Here, a very effective method for processing graphene from graphite using electrolytic exfoliation for mass production is presented. In addition, by using waste whey as an electrolyte in the study, the cost was reduced, and the presence of harmful chemicals was reduced. A simple and cost-effective exfoliation method has been demonstrated to prepare graphene forming a stable dispersion in the waste solvent, without any functionalization and surfactant. It has been observed that wastewater stored at +4 degrees helps EE due to its acidic nature. The existence of the produced graphene was successfully confirmed by XRD. The findings suggest a low-cost production process for synthesizing graphene and graphene oxide.

2. Material and Method

Materials and characterization

Two graphite rods with a diameter of 5.6 mm. Sodium sulphate Na_2SO_4 were supplied by Merck assay and used as electrolytes. All of the synthesis procedures involved the use of distilled water. The two electrodes received a DC voltage of 10 V as a constant potential (NEL Electronic). XRD measurements were performed on a Rigaku diffractometer X-ray Miniflex 600 model to identify the crystallographic structure of the graphene.

Graphene synthesis by electrochemical exfoliation

Figure 1 shows a schematic illustration of graphite EE. All experiments were carried out under ambient conditions. In this work, graphene was electrochemically synthesized using a traditional two-graphite rod electrode setup [14]. The wastewater whey to be used as the electrolyte in the experiment was filtered with qualitative filter paper to separate it from sediments. A graphite rod served as the working electrode and a second graphite rod served as the counter electrode for the EE. At a distance of around 2 cm, the anode and cathode graphite rods were positioned parallel to one another. A 100 ml solution of waste cheese water (+4 °C) and 10 g Na_2SO_4 (v/v) were used as the electrolyte. For one hour, the direct current (DC) bias voltage was maintained at 10 V. After the exfoliation process, 1 hour, the experimental setup was

turned off. The liquid part of the resulting graphene solution was poured, and the filtrate was centrifuged with distilled water at 1500 rpm for 5 minutes at room temperature three times. Following drying at 100 °C in a vacuum oven, the powder was produced [15]. During the entire electrochemical process, the release of gas bubbles was observed, which became denser with increasing electrolyte concentration. Figure 2 shows photographs of wastewater and the experimental setup.

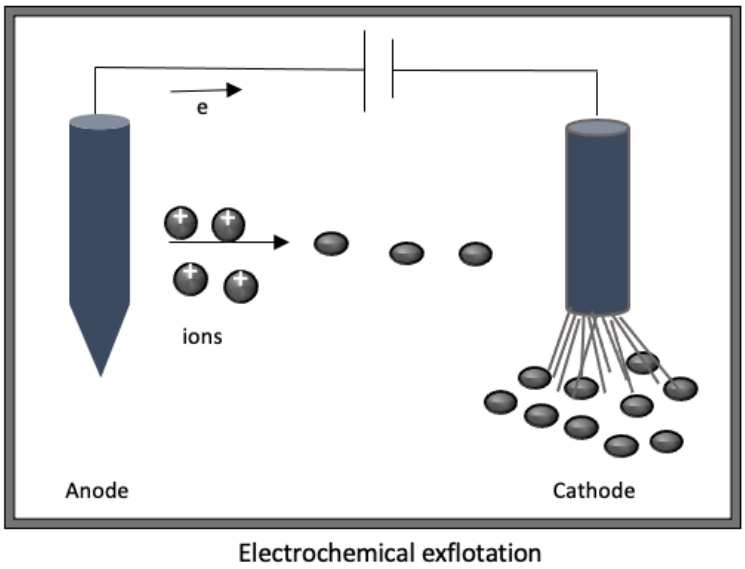

Figure 1. Diagram showing the equipment used in the electrolytic exfoliation method to synthesize graphene

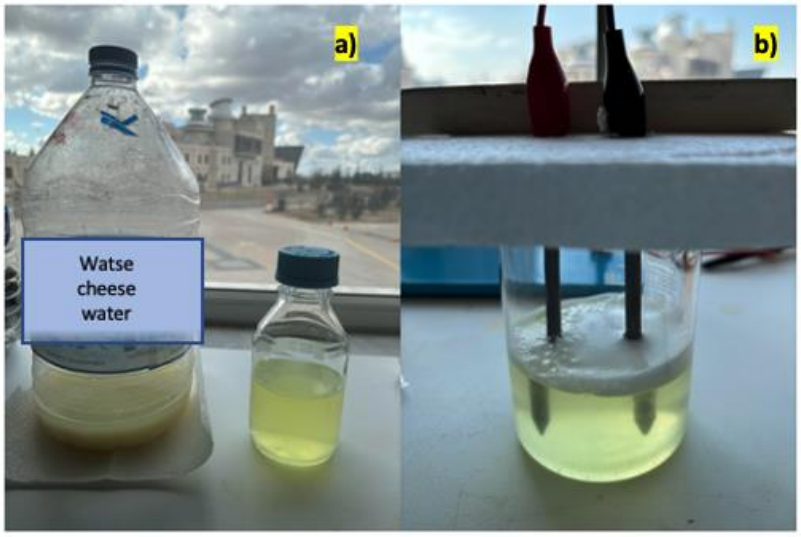

Figure 2. Photographs of (a) waste cheese water and (b) experimental setup

3. Result

The anode and cathode were separated by 2 cm and submerged in electrolyte to a depth of 100 mm prior to the electrical power being turned on [1]. Throughout the preparation process, it was noted that the electric current fluctuated but the voltage remained steady at 10 V. After electrolysis, a stable graphene dispersion was produced. To get bulk graphene particles, this supernatant was rinsed with DI water and then dried in a vacuum oven. Then, powder graphenes were analyzed by taking 5 g samples. Figure 3 shows the images of the anode and cathode electrodes before and after the electrolytic exfoliation reaction. It is clearly seen that the working area is corroded after the electrolytic exfoliation reaction of the graphite cathode electrode. Figure 4 images of the dispersion in the cell after the electrolytic exfoliation reaction (b) of the graphene dispersion after centrifugation are shown. Gas evolution was observed in the two-electrode cell. The graphene shed during the reaction accumulated at the bottom of the cell. After centrifugation, the graphene dispersion was overdried at 100 °C overnight to remove water.

Figure 3. Image of (a) anode and cathode electrodes before and (b) cathode electrodes after electrolytic exfoliation reaction

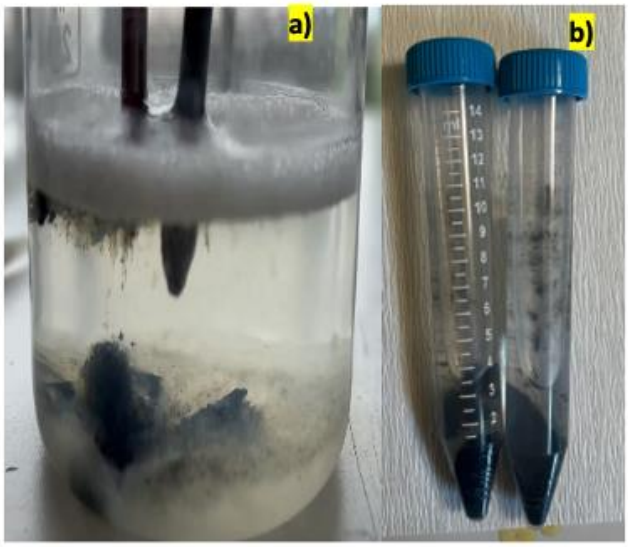

Figure 4. Photographs of (a) the graphene dispersion obtained by electrolytic exfoliation of graphite, (b) the state of the graphene dispersion after centrifugation

XRD was used to determine the exfoliated graphene's crystal structure and interlayer spacing. Three strong peaks at around 26.488°, 42°, and 54.5433°, which correspond to the (0 0 2), (1 0 1), and (0 0 4) crystallographic planes, respectively, are shown in Figure 5, which depicts the purification of the raw graphite powder [6]. The peak at $2\theta = 26°$, which corresponds to the (0 0 2) reflection of the graphitic structure and indicates the existence of graphene, is a hallmark interlayer stacking peak of aromatic systems [6, 12]. The XRD results, which are consistent with earlier research, demonstrated that graphite may be successfully exfoliated to produce graphene [12]. Figure 6 shows a Short Circuit Current versus time graph. In Figure 6 it can be seen that the current was at 0.36 when the experiment started. Meanwhile, the electrons released from the graphite anode began to move towards the cathode. After 5 minutes, this value reached the maximum value of 0.42. After 30 minutes, the current started to decrease and after an hour it dropped to 0.18.

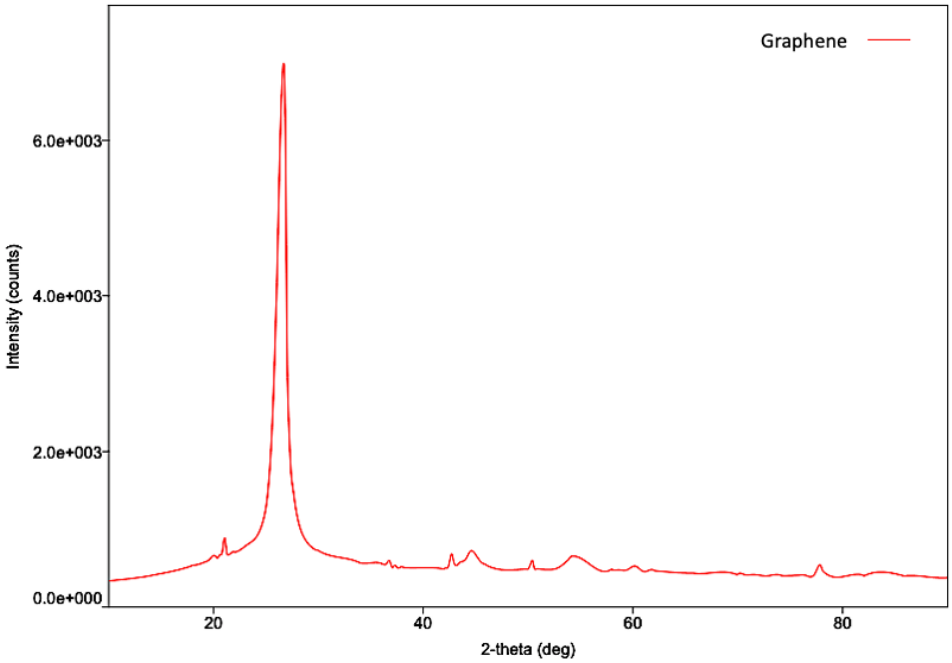

Figure 5. XRD spectrum of graphene

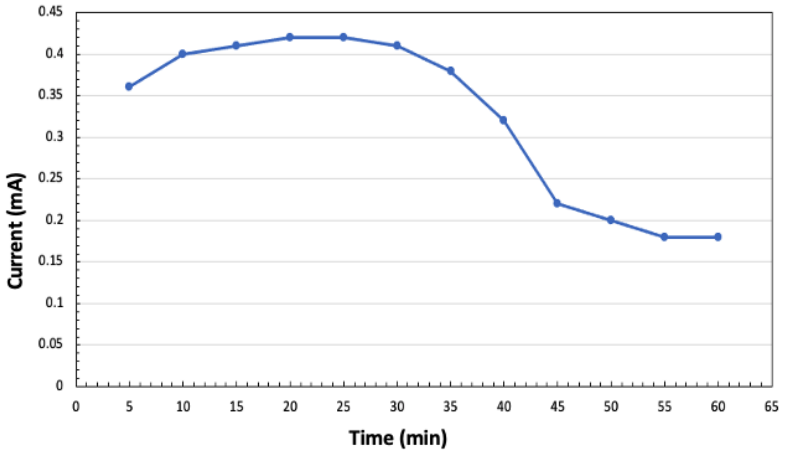

Figure 6. Current versus time graph

4. Discussion and Conclusion

In this work, leftover whey was used as the electrolyte in an extremely straightforward and inexpensive approach devised by EE to synthesize graphene from graphite rod. The exfoliation process was initiated by the wastewater weakening the bonding and interlayer forces inside the graphite during the effective reaction that occurred in the electrochemical cell. Graphene production was successfully achieved by 1-hour EE using a two-electrode arrangement at +10 V constant potential. Produced graphene can be used in various applications, especially energy applications. However, more experiments and characterizations are needed, and the electrolyte solution needs to be improved to achieve a more efficient reaction. Additionally, the study performed with two electrodes can be compared with a three-electrode cell. Thus, the usability of the graphene produced for supercapacitors and batteries can be discussed.

Conflict of Interest

All authors certify that they have no affiliations with or involvement in any organization or entity with any financial interest or non-financial interest in the subject matter or materials discussed in this manuscript.

Ethics Committee Approval

Ethics committee approval is not required.

Author Contribution

Conceptization, methodology, laboratory analyzes, writing draft, proof reading and editing: GBT.

Acknowledgements

The author thank the editors and reviewers for their critical remarks and suggestions during the preparation of the manuscript.

5. References

[1] Sun, H., Xu, G., Lian, W., Kastiukas, G., Zhang, J., Zhang, X., Liu, W., Xing, F., & Ren, J. (2022). Electrochemical synthesis and property characterisation of graphene oxide using water as electrolyte. *Chemical Physics Letters*, *786*, 139206.

[2] Yu, P., Lowe, S. E., Simon, G. P., & Zhong, Y. L. (2015). Electrochemical exfoliation of graphite and production of functional graphene. *Current Opinion in Colloid & Interface Science*, *20*(5–6), 329–338.

[3] Liu, F., Wang, C., Sui, X., Riaz, M. A., Xu, M., Wei, L., & Chen, Y. (2019). Synthesis of graphene materials by electrochemical exfoliation: Recent progress and future potential. *Carbon Energy*, *1*(2), 173–199.

[4] Singh, R. (2021). Recent progress in the electrochemical exfoliation of colloidal graphene: A Review. *Colloids - Types, Preparation and Applications*.

[5] Shabbir, M. K., Akhtar, J., Thebo, K. H., & Kazi, M. (2024). Synthesis of highly efficient ternary phase graphene/bi/SNO2 photocatalyst for degradation of organic dye pollutants. *Optik*, *304*, 171734.

[6] Htwe, Y. Z. N., Chow, W. S., Suda, Y., Thant, A. A., & Mariatti, M. (2019). Effect of electrolytes and sonication times on the formation of graphene using an electrochemical exfoliation process. *Applied Surface Science*, *469*, 951–961.

[7] Coroş, M., Pogăcean, F., Roşu, M.-C., Socaci, C., Borodi, G., Mageruşan, L., Biriş, A. R., & Pruneanu, S. (2016). Simple and cost-effective synthesis of graphene by electrochemical exfoliation of graphite rods. *RSC Advances*, *6*(4), 2651–2661.

[8] Wang, G., Wang, B., Park, J., Wang, Y., Sun, B., & Yao, J. (2009). Highly efficient and large-scale synthesis of graphene by electrolytic exfoliation. *Carbon*, *47*(14), 3242–3246.

[9] Yang, S., Brüller, S., Wu, Z.-S., Liu, Z., Parvez, K., Dong, R., Richard, F., Samorì, P., Feng, X., & Müllen, K. (2015). Organic radical-assisted electrochemical exfoliation for the scalable production of high-quality graphene. *Journal of the American Chemical Society*, *137*(43), 13927–13932.

[10] Yang, Y., Wang, Z., & Zheng, S. (2021). Secondary exfoliation of electrolytic graphene oxide by ultrasound assisted microwave technique. *Nanomaterials*, *12*(1), 68.

[11] Coroş, M., Pogăcean, F., Măgeruşan, L., Roşu, M.-C., Porav, A. S., Socaci, C., Bende, A., Stefan-van Staden, R.-I., & Pruneanu, S. (2018). Graphene-porphyrin composite synthesis through graphite exfoliation: The electrochemical sensing of Catechol. *Sensors and Actuators B: Chemical*, *256*, 665–673.

[12] Hamra, A. A. B., Lim, H. N., Chee, W. K., & Huang, N. M. (2016). Electro-exfoliating graphene from graphite for direct fabrication of Supercapacitor. *Applied Surface Science*, *360*, 213–223.

[13] Marković, Z. M., Budimir, M. D., Kepić, D. P., Holclajtner-Antunović, I. D., Marinović-Cincović, M. T., Dramićanin, M. D., Spasojević, V. D., Peruško, D. B., Špitalský, Z., Mičušik, M., Pavlović, V. B., & Todorović-Marković, B. M. (2016). Semi-transparent, conductive thin films of electrochemical exfoliated graphene. *RSC Advances*, *6*(45), 39275–39283.

[14] Fang, S., Lin, Y., & Hu, Y. H. (2019). Recent advances in green, safe, and fast production of graphene oxide via electrochemical approaches. *ACS Sustainable Chemistry & Engineering*, *7*(15), 12671–12681.

[15] Su, C.-Y., Lu, A.-Y., Xu, Y., Chen, F.-R., Khlobystov, A. N., & Li, L.-J. (2011). High-quality thin graphene films from fast electrochemical exfoliation. *ACS Nano*, *5*(3), 2332–2339.

doi:10.55385/kastamonujes.1483396 KUJES 10(1):44-51, 2024

Kastamonu University
Journal of Engineering and Sciences
e-ISSN 2667-8209
http://dergipark.gov.tr/kastamonujes

Evaluation of As, Cd, Ni and Se Content of Some Mineral Concrete Agents

Ibrahim Saleh Ibrahim Elajail[a, *], **Hakan Şevik**[b]

[a] Kastamonu University, Institute of Science, Department of Material Science and Engineering, Kastamonu, Türkiye
[b] Kastamonu University, Faculty of Engineering and Architecture, Department of Environmental Engineering, Kastamonu, Türkiye
***Corresponding Author:** hsevik@kastamonu.edu.tr

Received: **May 13, 2024** ◆ Accepted: **June 22, 2024** ◆ Published Online: **June 28, 2024**

Abstract: In this study, the variation of arsenic (As), cadmium **(**Cd), nickel **(**Ni) and selenium **(**Se) concentrations in some materials used as concrete admixtures were evaluated. These heavy metals are extremely hazardous elements for both human and other living organisms and the environment. Due to these hazards, they are on the priority pollutant list of both ATSDR and EPA. Study results show that heavy metal concentrations in some additives are at very high levels. As a result of the study, the highest As concentrations were obtained in copper slag, vermiculite and cem III cement, the highest Cd concentrations in crushed stone and copper slag, the highest Ni concentrations in copper slag, wood ash and brick powder, and the highest Se concentrations in blast furnace slag and cem III cement. This may pose a great risk to the health of people working in the industry and the environment.

Keywords: Concrete, additive, heavy metals

Öz: Bu çalışmada beton katkı maddesi olarak kullanılan bazı malzemelerdeki arsenik (As), kadmiyum (Cd), nikel (Ni) ve selenyum (Se) konsantrasyonlarının değişimi değerlendirilmiştir. Bu ağır metaller hem insan hem de diğer canlı organizmalar ve çevre için son derece tehlikeli elementlerdir. Bu tehlikeler nedeniyle hem ATSDR hem de EPA'nın öncelikli kirletici listesinde yer almaktadırlar. Çalışma sonuçları bazı katkı maddelerindeki ağır metal konsantrasyonlarının çok yüksek seviyelerde olduğunu göstermektedir. Çalışma sonucunda en yüksek As konsantrasyonları bakır cürufu, vermikülit ve cem III çimentosunda, en yüksek Cd konsantrasyonları kırmataş ve bakır cürufunda, en yüksek Ni konsantrasyonları bakır cürufu, odun külü ve tuğla tozunda, en yüksek Ni konsantrasyonları ise bakır cürufu, odun külü ve tuğla tozunda elde edildi. yüksek fırın cürufu ve cem III çimentosunda en yüksek Se konsantrasyonları. Bu durum endüstride çalışan insanların ve çevrenin sağlığı açısından büyük bir risk oluşturabilir.

Anahtar Kelimeler: Beton, katkı maddesi, ağır metaller

1. Introduction

The world population has now exceeded 8 billion and the proportion of the population living in urban areas has exceeded 50%. By 2030, it is estimated that the world population will exceed 8.5 billion and the proportion of the population living in urban areas may reach 90% [1-3]. Studies reveal that the most important global problems today are global climate change [4], urbanization [5] and environmental pollution [6].

Population growth and the concentration of population in urban areas cause a significant increase in the number of people living per unit area. Therefore, the construction of high-rise buildings in urban areas, which allow more people to live in the unit area, becomes compulsory [7, 8]. The basic building block of most of these buildings is concrete [9]. Today, concrete is the most consumed building material after water [10].

Concrete is also one of the most important expense items of construction costs. In order to reduce concrete costs, the use of various substances as concrete admixtures has become quite widespread [11, 12]. In recent years, many studies have been conducted on the use of various wastes generated as a result of production activities in other sectors as concrete admixtures. The use of these materials as concrete admixtures not only reduces concrete costs but also contributes significantly to the reduction of environmental pollution [13, 14].

Therefore, the use of various waste materials as concrete admixtures is one of the most important research topics. However, there is a significant lack of information on the chemical composition of these admixtures [15]. The lack of sufficient data on the chemical structure of concrete admixtures leads to a lack of information on the environmental effects of construction activities as well as the health of people working in the sector. In this study, it was aimed to determine the As, Cd, Ni and Se contents of some admixtures used as concrete admixtures, which are extremely harmful for human and environmental health. Since these metals are extremely harmful to human and environmental health, they are included in

the priority pollutant list of both US Environmental Protection Agency (EPA) and Agency for Toxic Substances and Disease Registry (ATSDR) [16].

Within the scope of the study, the concentrations of As, Cd, Ni and Se in some admixtures used as concrete admixtures were evaluated. The elements subject to the study are among the elements that are extremely dangerous for human and environmental health. In recent years, international health organizations have been classifying elements according to their hazards. In the studies conducted, ATSDR (Agency for Toxic Substances and Disease Registry) included 23 elements in the priority pollutant list due to their potential harm to humans and the environment. These elements are Ag, Al, As, Ba, Be, Cd, Co, Cr, Cu, Pb, Mn, Hg, Ni, Pd, Pu, Sb, Se, Sr, Tl, Th, U, V and Zn (28). Another important organization, EPA (U.S. Environmental Protection Agency) has defined Sb, As, Be, Cd, Cr, Cu, Pb, Hg, Ni, Se, Ag, Ti and Zn as Priority Pollutant Metals. The elements subject to the study are on both ATSDR and EPA's list of priority pollutants.

2. Material and Method

Within the scope of the study, it is aimed to determine the As, Cd, Ni and Se contents of some concrete mineral admixtures. For this purpose, samples were taken from these materials. Some of these materials are waste materials that are environmental pollution factors. The admixtures used within the scope of the study are as follows:

Table 1. Some of waste materials

No	Code	Material Names
M1	GDA	Recycling aggregate
M2	YFC	Blast furnace slag
M3	UCK	Fly ash
M4	KRC	Lime
M5	ODK	Wood ash
M6	ALC	Plaster
M7	KMT	Crushed Stone
M8	PMZ	Pumice
M9	TBK	Bottom ash
M10	SKU	Silica sand
M11	TGT	Brick powder
M12	SLD	Silica fume
M13	BKC	Copper slag
M14	CII	Cem II Cement
M15	VKL	Vermiculite
M16	CIV	Cem IV Cement
M17	DYT	Diatomite
M18	CIII	Cem III Cement
M19	CI	Cem I Cement
M20	LST	Tire powder
M21	MMT	Marble powder
M22	ZEO	Zeolite
M23	PRL	Perlite
M24	KRP	Red pumice

The materials obtained within the scope of the study were ground, sieved, then kept under laboratory conditions for two weeks until room dry and then placed in glass petri dishes and dried in an oven at 45 °C for two weeks. From the dried samples, 0.5 g of the sample was weighed and placed in tubes designed for microwave and 10 ml of 65% HNO_3 and 2 ml of 30% H_2O_2 were added. The prepared samples were incinerated in a specially designed microwave device at 280 PSI pressure and 180 ºC for 20 minutes. After the tubes removed from the microwave were cooled, deionized water was added and filled to 50 ml. The samples were filtered through filter paper and read at appropriate wavelengths in ICP-OES (Inductively Coupled Plasma-Optical Emission Spectrometry). This method is one of the most frequently used methods for elemental determination in recent years and is also used to determine the elemental content of concrete admixtures [15]. In the study, all measurements were performed in triplicate and the results of the study were evaluated at ppb level for higher sensitivity. The data obtained were evaluated by applying analysis of variance and Duncan test using SPSS 22.0 package program.

3. Findings

The variation of As, Cd, Ni and Se concentrations in the materials subject to the study on the basis of materials and statistical analysis results are given in Table 2.

Table 2. Statistical analy**sis** of As, Cd, Ni and Se concentrations

Materials	As (ppb)	Cd (ppb)	Ni (ppb)	Se (ppb)
GDA	55.585,3 de	906,2 m	9.616,9 g	8.810,2 g
YFC	1.973.397,5 n	268,0 a	3.304 c	44.326,3 s
UCK	197.070 j	478,7 de	13.272,8 h	9.441,1 h
KRC	7.541,2 a	457,7 cd	24.380,7 k	7.672,7 f
ODK	506.635 k	791,8 k	99.194,4 t	12.482,7 i
ALC	24.502,2 b	469,8 cde	3.960,1 cd	5.927,3 d
KMT	5.897,3 a	1.461,8 n	3.863,8 cd	6.684,8 e
PMZ	58.250,6 e	472,1 de	5.795,6 e	8.765,3 g
TBK	90.198,3 g	488,5 de	14.820,3 i	9.339,1 h
SKU	3.822,3 a	523,2 f	8.374,8 f	4.138,8 c
TGT	49.453,3 cd	759,1 j	71.638,3 s	27.996,3 n
SLD	9.510,3 a	563,6 g	3.665,8 c	2.546,8 b
BKC	1.385.854,2 m	1.441,6 n	366.595,0 u	36.968,8 r
CII	73.646,1 f	823,8 l	37.284,4 n	19.149,2 k
VKL	636.816,7 l	563,3 g	17.241,1 j	32.074,3 o
CIV	148.853,2 i	625,8 h	25.231,1 l	19.462,5 k
DYT	42.243,7 c	501,9 ef	53.682,3 r	16.887,9 j
CIII	2.102.506,7 o	460,8 cd	31.677 m	45.300,9 t
CI	150.669 i	748,9 j	39.361,6 o	26.070,8 m
LST	8.490,4 a	755,1 j	4.473,8 d	2.831,5 b
MMT	5.226,9 a	735,3 j	2.644,7 b	5.904,3 d
ZEO	112.339,9 h	367,8 b	4.531,9 d	22.887,7 l
PRL	6.944,8 a	437,7 c	1.603,8 a	1.929 a
KRP	154.639,3 i	677,5 i	4.0309 p	34.338,5 p
F value	6.458,779***	758,926***	103.658,039***	7517,605***

p<0,001=%99,9 p<0,01=%99 p<0,05=%95 p>0,05=ns

When the results of the table are analyzed, it is seen that the variation of As, Cd, Ni and Se on the basis of materials is statistically significant at 99.9% confidence level (p<0.001). As a result of Duncan test, it was determined that the materials formed 15 groups for As, 14 groups for Cd, 20 groups for Ni and 19 groups for Se. The graph showing the change in As concentration on the basis of materials is given in Figure 1

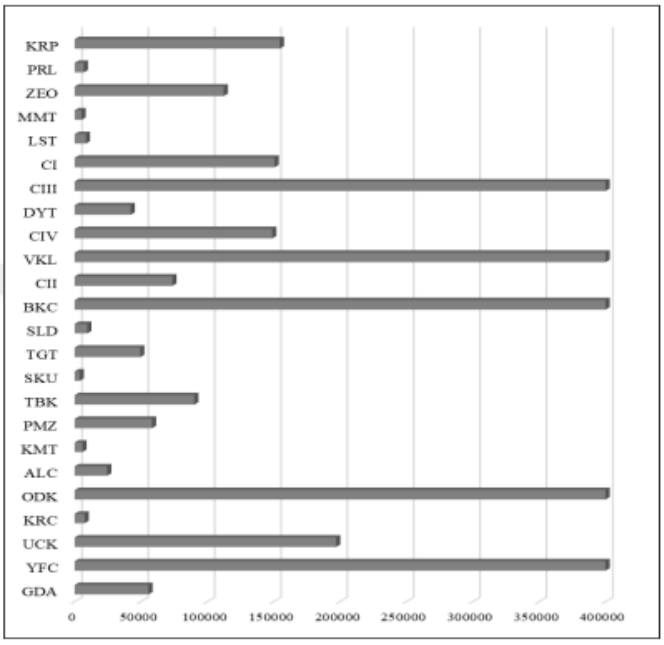

Figure 1. Variation of As (ppm) concentration by materials

Figure 1 shows that As concentration varies between 2,102,506.7 ppb and 3,822.3 ppb. The lowest values were obtained in SKU (3,822.3), MMT (5,226.9) and KMT (5,897.3), while the highest values were obtained in YFC (1,973,397.5), ODK (506,635), BKC (1,385,854.2), VKL (636,816.7) and CIII (2,102,506.7). When the values are analyzed, it is determined that there is approximately 550-fold difference between the lowest value and the highest value. Looking at the graph, the values were generally below 150,000 ppb. Only YFC (1,973,397.5), UCK (197,070), ODK (506,635), BKC (1,385,854.2), VKL (636,816.7), CIII (2,102,506.7) and KRP (154,639.3) exceeded this limit. The graph showing the variation of Cd concentration by materials is given in Figure 2.

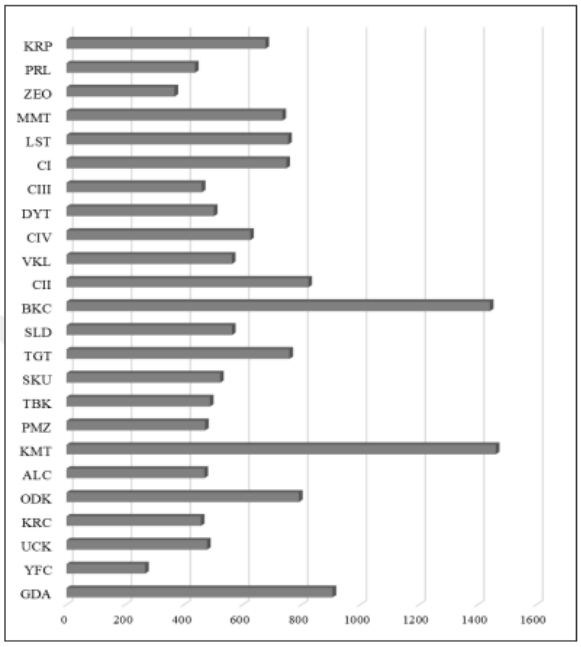

Figure 2. Variation of Cd (ppm) concentration by materials

Figure 2 shows that Cd concentration varied between 1,461.8 ppb and 268 ppb. The lowest values are observed in YFC (268.0) and ZEO (367.8), while the highest values are observed in KMT (1,461.8) and BKC (1441.6). When the values are analyzed, it is determined that 5.5 times the smallest value is equal to the largest value. When the graph is considered, it is seen that the values are generally below 600 ppb. Only GDA (906.2), ODK (791.8), KMT (1,461.8), TGT (759.1), BKC (1,441.6), CII (1,441.6), CIV (625.8), CI (748.9), LST (755.1), MMT (735.3) and KRP (677.5) were found to exceed this limit. The graph showing the variation of Ni concentration by materials is given in Figure 3.

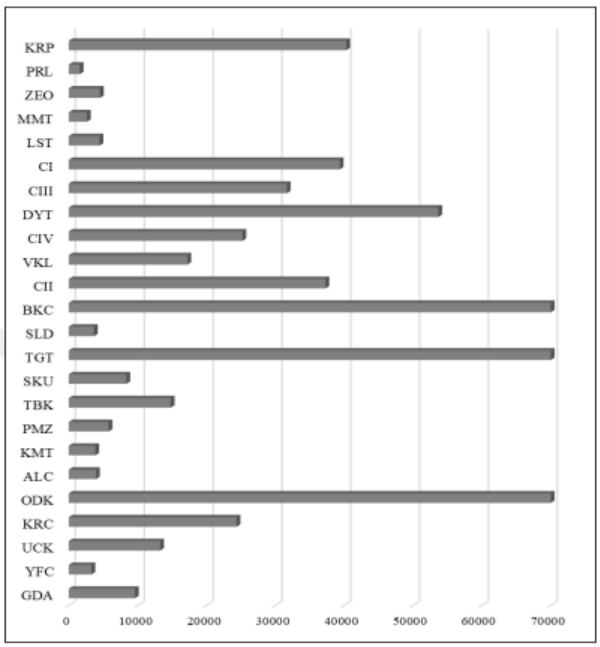

Figure 3. Variation of Ni (ppm) concentration by materials

Figure 3 shows that Ni concentration ranged between 366.595 ppb and 1.603,8 ppb. The lowest values were obtained in PRL (1.603,8), YFC (3.304), ALC (3.960,1), KMT (3.863,8) and MMT (2.644,7) while the highest values were obtained in BKC (366.595,0), ODK (99.194,4) and TGT (71.638,3). When the values were analyzed, it was determined that there was a difference of approximately 229 ppb between the lowest value and the highest value. In general, the values remained below 40,000 ppb. Only ODK (99,194.4), TGT (71,638.3), BKC (366,595.0) and DYT (53,682.3) exceeded this limit. The graph showing the variation of Se concentration by materials is given in Figure 4.

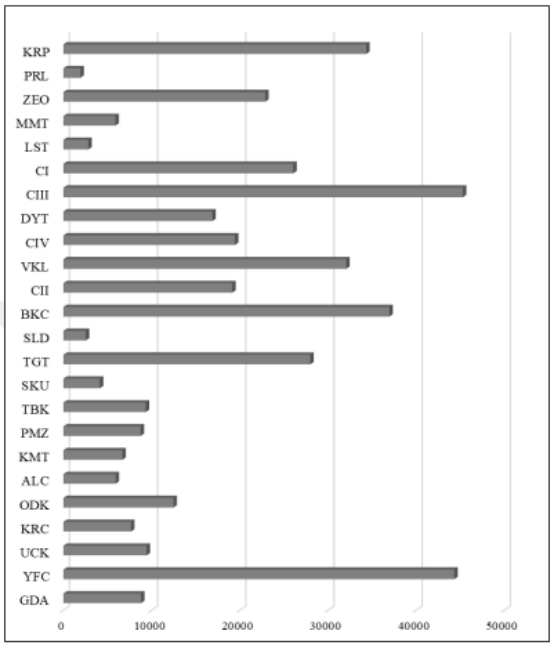

Figure 4. Variation of Se (ppm) concentration by materials

Figure 4 shows that Se concentration varied between 45,300.9 ppb and 1,929 ppb. The lowest values were obtained in PRL (1.929), LST (2.831,5) and SLD (2.546,8) while the highest values were obtained in YFC (44.326,3), TGT (27.996,3), BKC (36.968,8), VKL (32.074,3), CIII (45.300,9) and KRP (34.338,5). When the values were analyzed, it was determined that the lowest value was equal to the highest value of 23.5 ppb solid. Looking at the graph, the values were generally below 20,000 ppb. Only YFC (44,326.3), TGT (27,996.3), BKC (36,968.8), VKL (32,074.3), CIII (45,300.9), CI (26,070.8), ZEO (22,887.7) and KRP (34,338.5) exceeded this limit.

4. Results and Discussion

Heavy metals are elements whose concentrations in nature are constantly increasing, most of which are released into nature from anthropogenic sources such as mining, industry and traffic. They do not degrade or disappear easily in nature. Most of them are toxic, carcinogenic and fatal for living organisms even at low concentrations [17, 18]. Heavy metals, which are also the subject of this study, are elements that can pose a threat to human and environmental health even at low concentrations.

The values obtained as a result of the study may even exceed the values obtained in traffic and industrial zones, which are shown as the main sources of heavy metal pollution. For example, in a study conducted on road dust, it was determined that Cd concentration ranged between approximately 2.500 ppb and 4.500 ppb and Ni concentration ranged between 11.400 ppb and 22.400 ppb [19]. In this study, the concentrations obtained in some admixtures were much higher. According to these results, inhalation during the use of concrete admixtures may cause significant health risks. Because studies have shown that heavy metals are much more harmful if inhaled into the human body [3].

It is stated that construction activities, especially in urban centers, are one of the factors that most affect the amount of particulate matter in the air both during construction and demolition [15]. These particulate matter serve as a gathering center for heavy metals in urban areas. The chemical structure of particulate matter can also greatly affect heavy metal pollution in the air and subsequently in soil and water [20, 21]. Therefore, concrete admixtures can pose a major risk to the health of workers in construction activities. In addition, these particles may also adversely affect the health of people and living things living in urban areas.

Another striking result when the values obtained as a result of the study are examined is the differences between the lowest and highest values. For example, in As, one of the most harmful heavy metals for human health, there is approximately 550 times difference between the values obtained in the materials subject to the study. This result shows

that the chemical content of waste materials used as concrete admixtures can be very variable. Similar results were obtained for heavy metals such as Pb, Cr, Zn and Ba [15].

Heavy metal pollution is one of the most important environmental threats today [22, 23]. Environmental pollution is considered to be the most important problem on a global scale together with problems such as global climate change [24, 25] and urbanization [26-28]. The most important components of environmental pollution are heavy metals (11). Therefore, studies on monitoring and reducing heavy metal pollution are very current [29-32]. The results of the study reveal that the additives subject to the study contain high levels of heavy metals. The use of these substances will also contribute to the reduction of heavy metal pollution.

5. Conclusions

A total of 4 heavy metals were evaluated within the scope of the study. However, heavy metals such as Sb, Be, Ag and Cr, which are not subject to the study and are also included in the priority pollutant lists of organizations such as ATSDR and EPA, are also elements that pose a great risk to human and environmental health. Therefore, it is recommended that studies on the subject should be continued by diversifying and increasing, and other heavy metals should be subject to similar studies.

The materials subject to the study are waste materials and the use of these materials in recycling contributes significantly to reducing their environmental impact. Therefore, besides the use of these materials as concrete admixtures, their use in other areas should be investigated.

The heavy metals evaluated in this study are among the most dangerous heavy metals for human and environmental health. During the use of these substances as concrete additives, workers may be at great risk. Therefore, workers should be warned, necessary precautions should be taken and inspections should be carried out, especially when using heavy metals with high concentrations. Some of these materials are also used as raw materials in other sectors. Employees working in these sectors should also be warned and necessary precautions should be taken.

Conflict of Interest

All authors certify that they have no affiliations with or involvement in any organization or entity with any financial interest or non-financial interest in the subject matter or materials discussed in this manuscript.

Ethics Committee Approval

Ethics committee approval is not required.

Author Contribution

Conceptization: ISIE, HŞ; methodology and laboratory analyzes: ISIE, HŞ; writing draft: ISIE, HŞ; proof reading and editing: Other: All authors have read and agreed to the published version of manuscript.

Acknowledgements

Not appliable

6. References

[1] Worldometers, 2024. https://www.worldometers.info/

[2] Dogan, S., Kilicoglu, C., Akinci, H., Sevik, H., & Cetin, M. (2023). Determining the suitable settlement areas in Alanya with GIS-based site selection analyses. Environmental Science and Pollution research, 30(11), 29180-29189.

[3] Ghoma, W. E. O., Sevik, H., & kakaralar, K. (2023). Comparison of the rate of certain trace metals accumulation in indoor plants for smoking and non-smoking areas. Environmental Science and Pollution Research, 30(30), 75768-75776.

[4] Isinkaralar, O., Isinkaralar, K., Sevik, H., & Küçük, Ö. (2024). Spatial modeling the climate change risk of river basins via climate classification: a scenario-based prediction approach for Türkiye. Natural Hazards, 120(1), 511-528.

[5] Cetin, M., Sevik, H., Koc, I., & Cetin, I. Z. (2023). The change in biocomfort zones in the area of Muğla province in near future due to the global climate change scenarios. Journal of Thermal Biology, 112, 103434.

[6] Isinkaralar, O. (2024). QGIS-based modeling and analysis of urban dynamics affecting land surface temperature towards climate hazards in coastal zones of Portugal. Natural Hazards, 120(8), 7749-7764.

[7] Kaplan, G., Bayraktar, O. Y., Bayrak, B., Celebi, O., Bodur, B., Oz, A., & Aydin, A. C. (2023). Physico-mechanical, thermal insulation and resistance characteristics of diatomite and attapulgite based geopolymer foam concrete: Effect of different curing regimes. Construction and Building Materials, 373, 130850.

[8] Memiş, S., Yılmazoğlu, M. U., & Mütevelli, İ. G. (2016). Kastamonu İlinde Kullanılan Betonların Nicel Analizi. Düzce Üniversitesi Bilim ve Teknoloji Dergisi, 4(2), 756-764.

[9] İnce, G. Ç., & Yılmazoğlu, M. U. (2021). Probabilistic seismic hazard assessment of Muğla, Turkey. Natural Hazards, 107(2), 1311-1340.

[10] Isinkaralar, O., & Isinkaralar, K. (2023). Projection of bioclimatic patterns via CMIP6 in the Southeast Region of Türkiye: A guidance for adaptation strategies for climate policy. Environmental Monitoring and Assessment, 195(12), 1448.

[11] Sevik, H., Yıldız, Y., Özel, H.B. (2024). Phytoremediation and Long-term Metal Uptake Monitoring of Silver, Selenium, Antimony, and Thallium by Black Pine (Pinus nigra Arnold)" Bioresources, 19(3)

[12] Bayraktar, O. Y., Saglam-Citoglu, G., & Abo Aisha, A. E. S. (2019). The use of scrap tires in the construction sector. International Journal of Trend in Research and Development, 6(1), 253-256.

[13] Işınkaralar, K. (2020). Removal of formaldehyde and BTEX in indoor air using activated carbon produced from horse chestnut (Aesculus Hippocastanum L.) Shell. Ph.D. Thesis Hacettepe University, Institute of Science and Engineering, Department of Environmental Engineering. Ankara, Türkiye

[14] Isinkaralar, K. (2022). Some atmospheric trace metals deposition in selected trees as a possible biomonitor. Romanian Biotechnological Letters, 27(1), 3227-3236.

[15] Elajail, I. S. I., Sevik, H., Ozel, H. B., & Isik, B. (2022). Examining the chemical compositions of mineral concrete agents in terms of their environmental effects. Fresenius Environmental Bulletin, 31(9), 9784–9790

[16] Savas, D. S., Sevik, H., Isinkaralar, K., Turkyilmaz, A., & Cetin, M. (2021). The potential of using Cedrus atlantica as a biomonitor in the concentrations of Cr and Mn. Environmental science and pollution research, 28(39), 55446-55453.

[17] Yilmazoglu, M. U., & Ozocak, A. (2023). Bearing Capacity of Shallow Foundations on Unsaturated Silty Soils. Applied Sciences, 13(3), 1308.

[18] Özel, H. B., Şevik, H., Yıldız, Y., & Çobanoğlu, H. (2024). Effects of Silver Nanoparticles on Germination and Seedling Characteristics of Oriental Beech (Fagus orientalis) Seeds. BioResources, 19(2).

[19] Kaplan, G., Bayraktar, O. Y., Li, Z., Bodur, B., Yılmazoglu, M. U., & Alcan, B. A. (2023). Improving the eco-efficiency of fiber reinforced composite by ultra-low cement content/high FA-GBFS addition for structural applications: Minimization of cost, CO2 emissions and embodied energy. Journal of Building Engineering, 76, 107280.

[20] Koksal, F., Bayraktar, O. Y., Bodur, B., Benli, A., & Kaplan, G. (2023). Insulating and fire-resistant performance of slag and brick powder based one-part alkali-activated lightweight mortars. Structural Concrete, 24(3), 3128-3146.

[21] Yaprak, H., Memis, S., Kaplan, G., Yilmazoglu, M. U., & Ozkan, I. G. M. (2018). Effects on compressive strenght of accelerated curing methods in alkali activated mortars. International Journal of Scientific and Technological Research, 4(5), 70-78

[22] Memiş, S., Mütevelli, İ. G., & Yılmazoğlu, M. U. (2016). Sinop İlinde Üretilen Hazır Betonların İstatistiksel Olarak Değerlendirilmesi. Engineering Sciences, 11(4), 83-92.

[23] Isinkaralar, K., Isinkaralar, O., Koç, İ., Özel, H. B., & Şevik, H. (2023). Assessing the possibility of airborne bismuth accumulation and spatial distribution in an urban area by tree bark: A case study in Düzce, Türkiye. Biomass Conversion and Biorefinery, 1-12.

[24] Arıcak, B., Cantürk, U., Koç, İ., Erdem, R., & Şevik, H. (2024). Shifts That May Appear in Climate Classifications in Bursa Due to Global Climate Change. Forestist

[25] Kaplan, G., & Bayraktar, O. Y. (2021). The effect of hemp fiber usage on the mechanical and physical properties of cement based mortars. Research on Engineering Structures & Materials, 7, 245-258.

[26] Bayraktar, O. Y., Yarar, G., Benli, A., Kaplan, G., Gencel, O., Sutcu, M., ... & Kadela, M. (2023). Basalt fiber reinforced foam concrete with marble waste and calcium aluminate cement. Structural Concrete, 24(1), 1152-1178.

[27] Turkoglu, M., Bayraktar, O. Y., Benli, A., & Kaplan, G. (2023). Effect of cement clinker type, curing regime and activator dosage on the performance of one-part alkali-activated hybrid slag/clinker composites. Journal of Building Engineering, 68, 106164.

[28] Isinkaralar, O., Isinkaralar, K., & Ambade, B. (2024). Assessment of societal health risks: Spatial distribution and potential hazards of toxic metals in street dust across diverse communities. Water, Air, & Soil Pollution, 235(5), 302.

[29] Isinkaralar, K., Isinkaralar, O., & Bayraktar, E. P. (2024). Ecological and Health Risk Assessment in Road Dust Samples from Various Land Use of Düzce City Center: Towards the Sustainable Urban Development. Water, Air, & Soil Pollution, 235(1), 84.

[30] Istanbullu, S. N., Sevik, H., Isinkaralar, K., & Isinkaralar, O. (2023). Spatial distribution of heavy metal contamination in road dust samples from an urban environment in Samsun, Türkiye. Bulletin of Environmental Contamination and Toxicology, 110(4), 78.

[31] Isinkaralar, O., Świsłowski, P., Isinkaralar, K., & Rajfur, M. (2024). Moss as a passive biomonitoring tool for the atmospheric deposition and spatial distribution pattern of toxic metals in an industrial city. Environmental Monitoring and Assessment, 196(6), 513.

[32] Koç, İ., Canturk, U., Isinkaralar, K., Ozel, H. B., & Sevik, H. (2024). Assessment of metals (Ni, Ba) deposition in plant types and their organs at Mersin City, Türkiye. Environmental Monitoring and Assessment, 196(3), 282.